

# The Śnieżka peatland as a candidate for the Global Boundary Stratotype Section and Point for the Anthropocene series

## Journal Article

**Author(s):**

Fiałkiewicz-Kozieł, Barbara; Łokas, Edyta; Smieja-Król, Beata; Turner, Simon; De Vleeschouwer, Francois; Woszczyk, Michał; Marcisz, Katarzyna; Gałka, Mariusz; Lamentowicz, Mariusz; Kołaczek, Piotr; Hajdas, Irka; Karpińska-Kołaczek, Monika; Kołtonik, Katarzyna; Mróz, Tomasz; Roberts, Sarah; Rose, Neil; Krzykawski, Tomasz; Boom, Arnoud; Yang, Handong

**Publication date:**

2023-04

**Permanent link:**

<https://doi.org/10.3929/ethz-b-000592360>

**Rights / license:**

[Creative Commons Attribution-NonCommercial 4.0 International](#)

**Originally published in:**

The Anthropocene Review 10(1), <https://doi.org/10.1177/20530196221136425>

# The Śnieżka peatland as a candidate Global boundary Stratotype Section and Point for the Anthropocene series

The Anthropocene Review

2023, Vol. 10(1) 288–315

© The Author(s) 2022





Article reuse guidelines:

[sagepub.com/journals-permissions](https://sagepub.com/journals-permissions)

DOI: 10.1177/20530196221136425

[journals.sagepub.com/home/anr](https://journals.sagepub.com/home/anr)



Barbara Fiałkiewicz-Kozieł,<sup>1</sup>  Edyta Łokas,<sup>2</sup>  
Beata Smieja-Król,<sup>3</sup> Simon Turner,<sup>4</sup> Francois De Vleeschouwer,<sup>5</sup>  
Michał Woszczyk,<sup>1</sup> Katarzyna Marcisz,<sup>6</sup> Mariusz Gałka,<sup>7</sup>  
Mariusz Lamentowicz,<sup>6</sup> Piotr Kołaczek,<sup>6</sup> Irka Hajdas,<sup>8</sup>   
Monika Karpińska-Kołaczek,<sup>6</sup> Katarzyna Kołtonik,<sup>2</sup> Tomasz Mróz,<sup>9</sup>  
Sarah Roberts,<sup>4</sup> Neil Rose,<sup>4</sup> Tomasz Krzykawski,<sup>3</sup> Arnoud Boom<sup>10</sup>  
and Handong Yang<sup>4</sup>

## Abstract

The subalpine, atmospherically fed Śnieżka peatland, located in the Polish part of the Sudetes, is one of the nominated candidates for the GSSP of the Anthropocene. Data from two profiles, Sn1 (2012) and Sn0 (2020), from this site are critical for distinguishing the proposed epoch, while an additional core Sn2 is presented to support main evidence. The Sn0 archive contains a wide array of critical markers such as plutonium (Pu), radiocarbon ( $F^{14}C$ ), fly ash particles, Hg and stable C and N isotopes which are consistent with the previously well documented  $^{210}Pb/^{14}C$  dated Sn1 profile, which provides a high-resolution and comprehensive database of trace elements and rare earth elements (REE), Pb isotopes, Pu, Cs, pollen and testate amoebae. The 1952 worldwide appearance of Pu, owing to its global synchronicity and repeatability between the cores, is proposed here as a primary marker of the Anthropocene, supported by the prominent upturn of selected chemostratigraphic and biostratigraphic indicators as well as the appearance of technofossils and artificial radionuclides.

<sup>1</sup>Adam Mickiewicz University, Poland

<sup>2</sup>IFJ, Polish Academy of Sciences, Poland

<sup>3</sup>University of Silesia, Poland

<sup>4</sup>University College London, UK

<sup>5</sup>Universidad de Buenos Aires, Argentina

<sup>6</sup>Adam Mickiewicz University, Poland

<sup>7</sup>University of Lodz, Poland

<sup>8</sup>ETH Zurich, Switzerland

<sup>9</sup>Jagiellonian University, Poland

<sup>10</sup>University of Leicester, UK

## Corresponding author:

B Fiałkiewicz-Kozieł, Adam Mickiewicz University, Faculty of Geographical and Geological Sciences, Institute of Geocology and Geoinformation, Biogeochemistry Research Unit, Krygowskiego 10, Poznań 61-680, Poland.  
Email: [basiafk@amu.edu.pl](mailto:basiafk@amu.edu.pl)

## Keywords

*Ambrosia artemisiifolia*, Great Acceleration, plutonium, SAP, SCP, stratotype of Anthropocene, testate amoebae, the Sudetes, trace elements

## Introduction

Peatlands cover around 2%–3% of the Earth continental surface (Xu et al., 2018) and, owing to sequestration/release of CO<sub>2</sub>, play a crucial role in the regulation of global climate (Gallego-Sala et al., 2018; Loisel et al., 2014; Yu, 2012). At the same time, peatlands are excellent repositories of past and recent environmental changes (De Vleeschouwer et al., 2010a; Shotyk, 1988). The stability of peatlands and their ability to accumulate carbon (C) is affected by climate, in particular air temperature and precipitation, atmospheric pollution, fire, sea level, permafrost thawing and land use (Loisel et al., 2021). Even though these factors operate on different temporal and spatial scales, the peatlands vulnerability to environmental change varies geographically (Turetsky et al., 2014). Millar et al. (2017) claimed that subalpine mires were more stable C reservoirs compared to lowland peatlands, and consequently, they provide highly reliable records of environmental changes (Rangwala and Miller, 2012), as confirmed by many studies (e.g. Bao et al., 2015; Fiałkiewicz-Kozieł et al., 2022; Hansson et al., 2017).

The Sudetes are a central European mountain range located between Poland and the Czech Republic, within the so-called Black Triangle, one of the most polluted areas of Europe (Figure 1). The subalpine Śnieżka peatland within the highest Karkonosze mountain range of the Sudetes provides an excellent opportunity to gain an insight into the long-ranged dispersal of transboundary traces of human activity and thus to investigate the negative human impact on the environment within the recent past.

Evidence of human activity in the Sudetes extends back to Palaeolithic settlements and later Neolithic agriculture (Valde-Novak, 1999). From the third century BCE, there is evidence of the exploitation of river-deposited gold by Celts (Woźniak, 1970). The intense mining of rich metal ores (gold and precious minerals) in the region commenced in the 12th century (Julkowska, 2016). By the 20th century, numerous mines, factories and power plants made the region one of the most polluted in Europe (Grübler, 2002; Kolář et al., 2015). In the 1970s, the synergistic impact of extremely high levels of acid rain, alkali ashes and insect outbreaks caused significant damage to coniferous forests in this area and directly affected human health (Mazurski, 1986). The signing of a joint declaration on cooperation in solving environmental problems in the Black Triangle by the German, former Czechoslovakian and Polish governments in 1991 prompted the improvement and protection of the area (Grübler, 2002; Kolář et al., 2015).

The unprecedented pollution level in the Sudetes region created a need for scientific assessment of the quality of the environment. The most severely affected Izery Mts range (Glina and Bogacz, 2012; Magiera et al., 2019; Zuna et al., 2011) received major attention. Since the time the problem was identified, many reports on acid rain (Mazurski, 1986), dust mineralogy, pollen analysis, sulphur and carbon isotopes (i.e. Kajukało et al., 2016; Popowski, 2005; Skrzypek et al., 2009; Speranza et al., 2000), magnetic susceptibility and geochemistry (i.e. Bińczycki et al., 2020; Fiałkiewicz-Kozieł et al., 2015; Strzyszczyk and Magiera, 2001), ecology and anthropopressure (Pech et al., 2022; Wojtuń et al., 2018) have been published.

However, the Śnieżka peatland (Sn) has the most comprehensive, high-resolution geochemical and palaeoecological record in the Sudetes. Concentrations of Pb, Zn, Cu, Ni, Cr, Ti, Al, U, Sc, rare earth elements (REE), mineralogy and <sup>204</sup>Pb, <sup>206</sup>Pb, <sup>207</sup>Pb, <sup>208</sup>Pb, <sup>234</sup>U, <sup>137</sup>Cs, <sup>239</sup>+<sup>240</sup>Pu have been determined (Fiałkiewicz-Kozieł et al., 2020). This study revealed the presence of both regional and

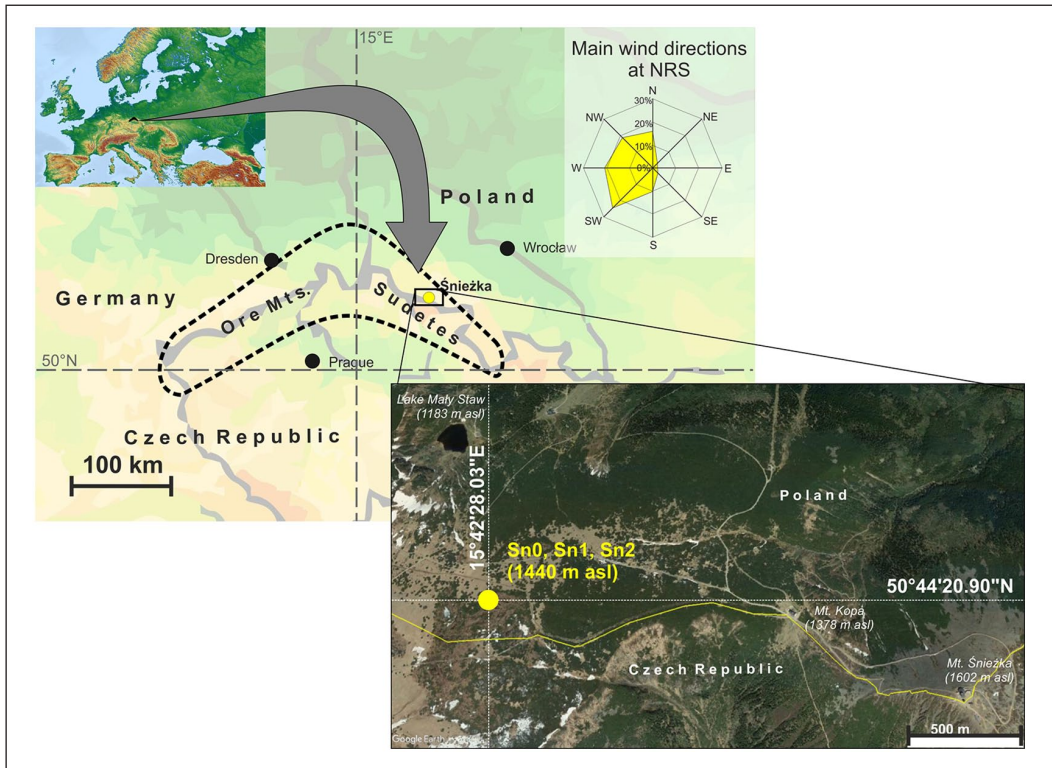


**Figure 1.** Map of the study site. The wind rose after Sobik et al. (2014). Reproduced in colour in online version.

global trends in the stratigraphic record, such as the combustion of fossil fuels, the catastrophic release of artificial radionuclides during the Chernobyl accident, and atmospheric nuclear weapon tests. The quality of the record was the basis for nominating the Śnieżka Peatland as a GSSP candidate for the Anthropocene series (AWG, 2020; Luciano, 2022).

The preparatory activities of the Anthropocene Working Group, including events leading to the submission of GSSP proposals and the binding decision that the base of the Anthropocene should align with stratigraphic signals dating to the mid-20th century, are detailed in the introductory article to this special issue (Waters et al., 2023).

This paper aims to review the geochemical and palaeoecological data from the Śnieżka candidate site. The data presented involves three cores (Sn0, Sn1 and Sn2). Special focus is placed on the Sn0 core (2020), which provides the most representative continuous record containing the possible GSSP. This is supported by additional detailed data from Sn1 (2012), and the summary is based on both profiles. Data from Sn2 (2012) are also presented to support these results.

## Materials and methods

### Geographic setting

The study site is located in the Polish part of the Sudetes mountains. The Śnieżka peatland (50°44'N, 15°42'E) is developed on a plateau (1440 m a.s.l.) in the Karkonosze range, close to the highest summit of Mt. Śnieżka (1602 m a.s.l.; Figure 1).



The mountain range is a significant orographic barrier for regional-continental air masses, and the dominated winds are westerlies (Sobik et al., 2014). For 64% of the year, the area is directly influenced by the zonal circulation of oceanic air masses from the North Atlantic, flowing over the lowlands of Western Europe. About 30% of the year is characterised by polar continental air masses flowing from the east, 4% by arctic air from the north and 2% by tropical air masses from the south (Sobik et al., 2014). The mean annual air temperature at Mt. Śnieżka, based on 1881–2012 measurements, is  $+0.5^{\circ}\text{C}$ . The lowest annual mean temperature of  $-1.2^{\circ}\text{C}$  was observed in 1941, and the highest value of  $+2.3^{\circ}\text{C}$  was registered in 2000, 2006 and 2011 (Urban and Tomczyński, 2017). The annual precipitation is  $\sim 1500\text{ mm}$  (Migała et al., 2016; Sobik et al., 2014). The present plant community of the peatland consists of *Sphagnum lindbergii*, *Sphagnum balticum*, *Carex limosa*, *Carex rostrata*, *Baeothryon caespitosum*, *Eriophorum vaginatum*, *Empetrum hermaphroditum*, *Andromeda polifolia*, *Oxycoccus palustris* and *Rubus chamaemorus* as well as dwarf *Pinus mugo* (Wojtuń, 2006).

### Sampling

Cores Sn1 and Sn2 (63 and 67 cm in length, respectively) were retrieved in the spring of 2012, and 50 cm long GSSP core – Sn0 was collected in the summer of 2020 using a stainless-steel  $10 \times 10 \times 100\text{ cm}$  Wardenaar corer (Wardenaar, 1987). The distance between all three cores is approximately 15 m (Sn0:  $50^{\circ}44'20,90''\text{N}$ ,  $15^{\circ}42'28,03''\text{E}$ ; Sn1:  $50^{\circ}44'21,40''\text{N}$ ,  $15^{\circ}42'28,23''\text{E}$ , Sn2:  $50^{\circ}44'20,67''\text{N}$ ,  $15^{\circ}42'29,44''\text{E}$ ). The monoliths were sealed in plastic bags, transported to the laboratory in Poznań (Adam Mickiewicz University – AMU) and stored in the laboratory fridge. Cores were cut into 1-cm thick slices (except the top 6 cm of Sn1 and Sn2, which were cut in 2-cm slices) using a carbon steel knife.

While Sn1 and Sn2 preparation followed the procedure described in Givelet et al. (2004) and De Vleeschouwer et al. (2010b), Sn0 was only partially subsampled, and a complete  $5\text{ cm} \times 5\text{ cm} \times 50\text{ cm}$  core is retained as an archive in a cold room ( $4^{\circ}\text{C}$ ).

### Methods

A concise summary of the applied methods is provided below. A detailed description of all methods can be found in Supplemental Material 1 and Fiałkiewicz et al. (2020) for Sn1 and Sn2. Physical properties and macrofossils were determined in every slice using standard methods (De Vleeschouwer et al., 2010b; Givelet et al., 2004). Activities of  $^{210}\text{Pb}$  and  $^{137}\text{Cs}$  were determined for each sub-sample of Sn0 by gamma-ray spectrometry using a high purity germanium detector (DSG, Germany) located at the Institute of Physics, Jagiellonian University. Measurements of  $^{238}\text{Pu}$ ,  $^{239}\text{Pu}$  and  $^{240}\text{Pu}$  activities were undertaken using an alpha-particle spectrometer (Alpa Analyst, Canberra) with semiconductor, passivated planar silicon detectors (PIPS, Canberra). Fourteen samples of macrofossils from core Sn0 were analysed at the AMS facility in ETH Zurich. After the Acid-Base-Acid treatment (Hajdas, 2008), samples were graphitised (Němec et al., 2010) and analysed using the MICADAS system (Synal et al., 2007). Total concentrations of elements (Sn1, Sn2) were measured using ICP-MS at the Adam Mickiewicz University (UAM) for trace metals and Observatoire Midi-Pyrénées (Toulouse, France) for Rare Earth Elements. Mercury (Hg) (Sn0) was measured using cold vapour-atomic fluorescence spectrometry (CV-AFS). The measurements of stable lead (Pb) isotopes (Sn1, Sn2) were conducted on TIMS Finnigan MAT-261 special (UAM). Total nitrogen (N), carbon (C) and sulphur (S) values (Sn2) were determined in dried and homogenised samples with a VarioMax CNS elemental analyser (Elementar Analysensysteme GmbH, Germany). CN, C and N isotopes (Sn0) were

analysed on an elemental analyser (ANCA GSL, Sercon, UK). SCPs (Sn0) were determined using light microscopy following the procedure of Rose (1994). Dust particles were determined (all three profiles) using the backscattered electron detector (BSE) of a scanning electron microscope (SEM) equipped with an energy-dispersive X-ray analysing system (SEM-FEI Quanta 250; University of Silesia in Katowice). Mullite content was determined in the profiles using X-ray diffraction (XRD), following the method described in Smieja-Król et al. (2019). Pollen and testate amoebae (Sn1) were determined using light microscopy following standard procedures. Non-metric multidimensional scaling (NMDS) was used to define the relationships between geochemical data, water table reconstruction and the response of testate amoeba and vegetation (pollen data) to anthropogenic forcing.

## Results

### *Physical properties and macrofossils (Sn0, Sn1, Sn2)*

The three investigated cores showed similar patterns of peat accumulation (Figure 2). Initially, the peat layers were mainly composed of minerotrophic mosses such as *Sphagnum russowii* and *Straminergon stramineum*, then followed by *Sphagnum lindbergii* in cores Sn1 and Sn2. In the upper part of the three peat monoliths, *Polytrichum strictum* also played a meaningful role as a peat-forming species. In the topmost part of Sn2 *S. medium/divinum* and *S. balticum* re-appeared, indicating a more oligotrophic habitat. Importantly, the preferred boundary of the proposed Anthropocene series is not encompassed by the boundary of local macrofossil zones. The detailed description of macrofossils can be found in the Supplemental Material 2.

The ash content (AC) in Sn0 and Sn1 is low (up to 6%) and shows more complex patterns compared to the botanical layering of peat. The Sn0 core has two zones with a boundary at c.a. 18 cm depth (Figure 2). The lower zone has 2%–4% higher ash content values than the upper one. In Sn1, there is a slight enrichment in AC between 36 and 22 cm. In this layer, AC is between 2% and 5% compared to <2% in underlying and overlying peat.

In Sn2, AC distribution shows considerable variability especially below 17.5 cm depth, where there are three positive excursions of AC at ca. 42.5, 32.5 and 28 cm. Above 17.5 cm two layers can be identified with enhanced (up to 6%) AC values between 17 and 10 cm and <3% contents in the topmost 10 cm.

Higher and more numerous maxima of AC in Sn2 indicated possible disturbance. Therefore, we used Sn2 only to show some critical results, such as mullite and SAP appearance, which correspond to the proposed Anthropocene series level within the geochemical profile (Figure 4).

### *Radioisotopes (Sn0, Sn1)*

Activity concentrations of  $^{137}\text{Cs}$  in both profiles (Sn0, Sn1) were comparable and ranged between  $56 \pm 2$  and  $2576 \pm 55$  Bq/kg (Figure 3). Most of the total Cs activity concentration in Sn1 is retained in the upper 9 cm-thick layer. Two distinct peaks of  $^{137}\text{Cs}$  activity can be found at 23.5 cm ( $1011 \pm 48$  Bq/kg) and 26.5 cm depth ( $699 \pm 58$  Bq/kg). These peaks act as lithochronohorizons for the Chernobyl accident (1986) and the atmospheric nuclear weapon tests (1963), respectively.

In the Sn0 profile, three characteristic maxima of  $^{137}\text{Cs}$  were observed. The uppermost was located just below the peat surface, albeit lower than in the Sn1. The second activity peak occurred between 17 and 20 cm (maximum at 17.5 cm) and can be related to the Chernobyl event (1986). The lowest Cs peak, at 27–29 cm, was assigned to the nuclear weapon tests (1963), which was corroborated by the nearby position of Pu maximum at 30.5 cm depth.

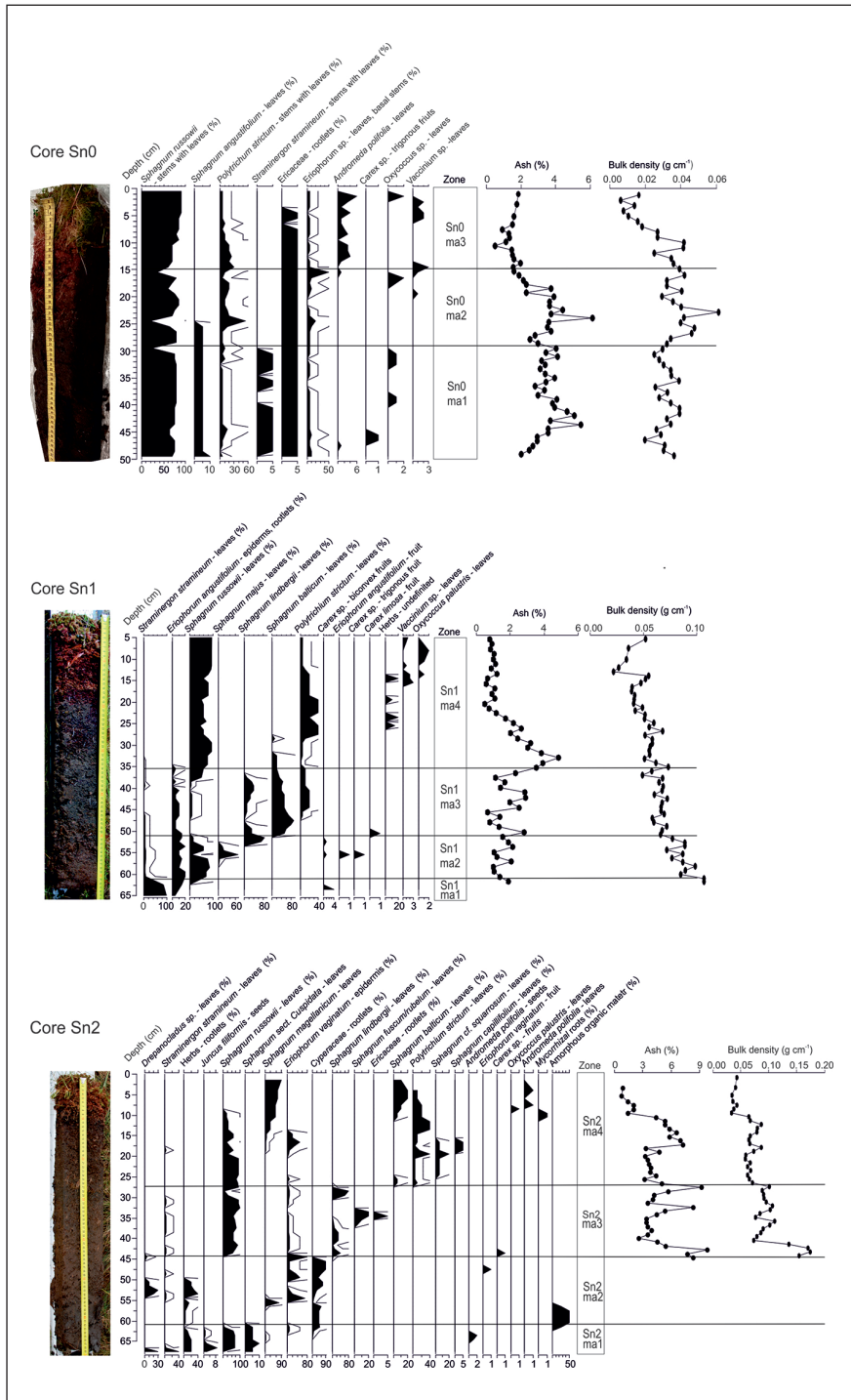


**Figure 2.** Results of macrofossil analysis and physical properties of peat profiles for all investigated cores. Reproduced in colour in online version.

The first traces of  $^{239+240}\text{Pu}$  occur at 45.5–46.5 cm depth in Sn1, with the maximum at 32.5–33.5 cm (Figure 3). The first distinct increase is recorded at a depth of 43.5–44.5 cm (Sn0), followed by a prominent peak at 30–31 cm depth, which correlates with the 1963 nuclear weapon tests. Above, the activity decreased continuously up-core until the next tiny peak recorded at 17.5–18.5 cm depth (Sn0) and 22.5–23.5 cm depth (Sn1), which correlates with the Chernobyl accident in 1986. The  $^{239+240}\text{Pu}$  activities then declined to minimum detectable activity (MDC) and varied between 0.04 and 0.09 Bq/kg in the upper part of the profiles Sn1 and Sn0.

Results of  $^{14}\text{C}$  in Sn0 samples are expressed as  $F^{14}\text{C}$  (fraction modern  $^{14}\text{C}$ ) (Reimer et al., 2004) and calibrated using the Bayesian sequence model of the OxCal calibration programme (Bronk Ramsey, 2009) with the bomb peak atmospheric data for the Northern Hemisphere (Hua et al., 2022). Except for one sample (Sn0 37.5 cm), all the samples follow the atmospheric NH bomb peak data (Supplemental Table 2; Figure 10). The high value of  $F^{14}\text{C}$  measured for sample Sn0 37.5 might be due to the intrusion of young material into the lower layers of sediment. Consequently, the sample was not included in the OxCal model.

$^{14}\text{C}$  modelling for Sn1 revealed 220 years of peat accumulation. The data obtained from  $^{14}\text{C}$  activity suggests a hiatus in the Sn2 profile. Therefore, for further interpretation, only the top 44 cm, which spans a similar time interval compared to Sn1, were used for interpretation.

### $^{210}\text{Pb}$ chronology (Sn0, Sn1)

The total  $^{210}\text{Pb}$  ( $^{210}\text{Pb}_{\text{tot}}$ ) activity concentration versus profile depth is presented in Supplemental Table 1. The supported part ( $^{210}\text{Pb}_{\text{sup}}$ ) was obtained as the mean value ( $\pm\text{SD}$ ,  $1\sigma$ ) of activities for the lowermost layers, where the level of  $^{210}\text{Pb}_{\text{tot}}$  has reached a steady value. By subtracting  $^{210}\text{Pb}_{\text{sup}}$  activity from  $^{210}\text{Pb}_{\text{tot}}$  activity on a level-by-level basis, the unsupported fraction ( $^{210}\text{Pb}_{\text{uns}}$ ) was calculated. The average value for  $^{210}\text{Pb}_{\text{sup}}$  fraction was the same for Sn0 and Sn1 and was estimated as  $16 \pm 3$  Bq/kg. Based on the CF/CS model applied to  $^{210}\text{Pb}$  activities, the bottom of Sn0 (50 cm) was dated to  $1931 \pm 8$  CE and the Sn1 (51 cm) was dated to  $1927 \pm 5$  CE. Thus, the cores encompassed  $90 \pm 8$  and  $86 \pm 5$  years, respectively. The linear accumulation rates in Sn0 and Sn1 were  $0.65 \pm 0.11$  and  $0.53 \pm 0.04$  cm/year, respectively, and the mass accumulation rate  $r$  was  $0.020 \pm 0.002$  and  $0.035 \pm 0.002$  g  $\text{cm}^2/\text{year}$ , respectively.  $^{210}\text{Pb}$ -derived dates from ombrotrophic peat deposits are always validated by independent evidence such as pollution records or other radioisotopes, including  $^{239+240}\text{Pu}$ ,  $^{241}\text{Am}$  (e.g. Appleby et al., 1997; Cwanek et al., 2021; Gallagher et al., 2001; MacKenzie et al., 1998) because decreasing with depth  $^{210}\text{Pb}$  activity provided older than expected data.  $^{210}\text{Pb}$  dating of peat has been suggested to be unreliable in some studies (e.g. Urban et al., 1990), especially when the CRS model is used (Cwanek et al., 2021; Mróz et al., 2017). Both models (CF=CRS and CF/CS) were used to calculate the ages, but the CRS model gave very old ages for the bottom layers ( $1828 \pm 10$  CE for 44.5 cm compared to CF/CS  $1941 \pm 7$  (Supplemental Table 1). For the peat layers dated with Pu at 1952 (the appearance of plutonium in the environment) in core Sn0 and Sn1, the CF/CS model gave  $1949 \pm 7$  CE and  $1948 \pm 4$  CE, while the CRS model provided much older dates of  $1900 \pm 2$  CE and  $1921 \pm 1$  CE, respectively. Similarly, the layers corresponding to the maximum of  $^{239,240}\text{Pu}$  concentrations reflecting the peak fallout of 1963 were better dated with the CF/CS model.

The main distinction between the two models is that CF/CS assumes a constant atmospheric flux of  $^{210}\text{Pb}$  to the peatland surface and a constant accumulation rate. In contrast, CRS assumes a constant atmospheric flux of  $^{210}\text{Pb}$  and a variable accumulation rate of peatlands (Supplemental Table 1, Figures 7 and 8).

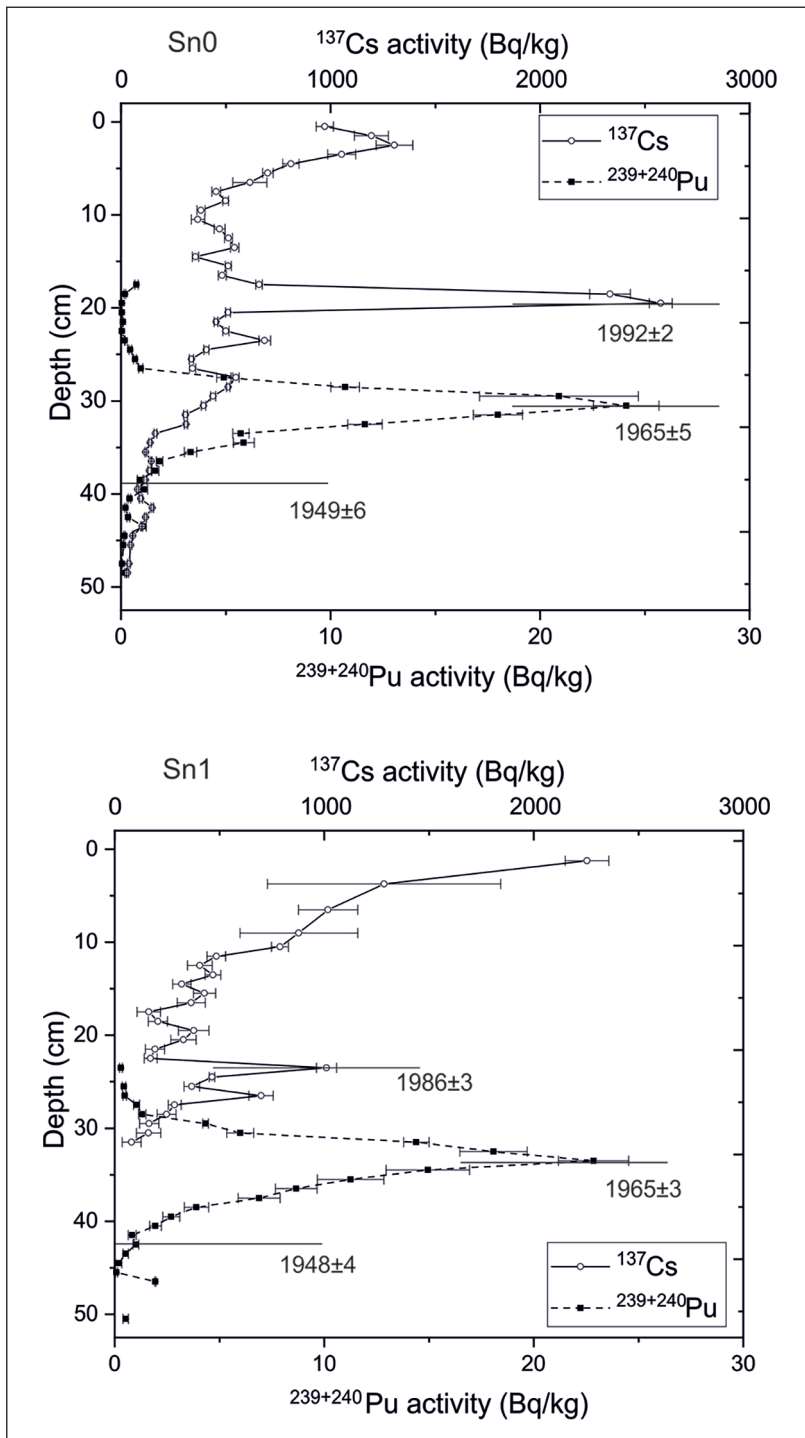
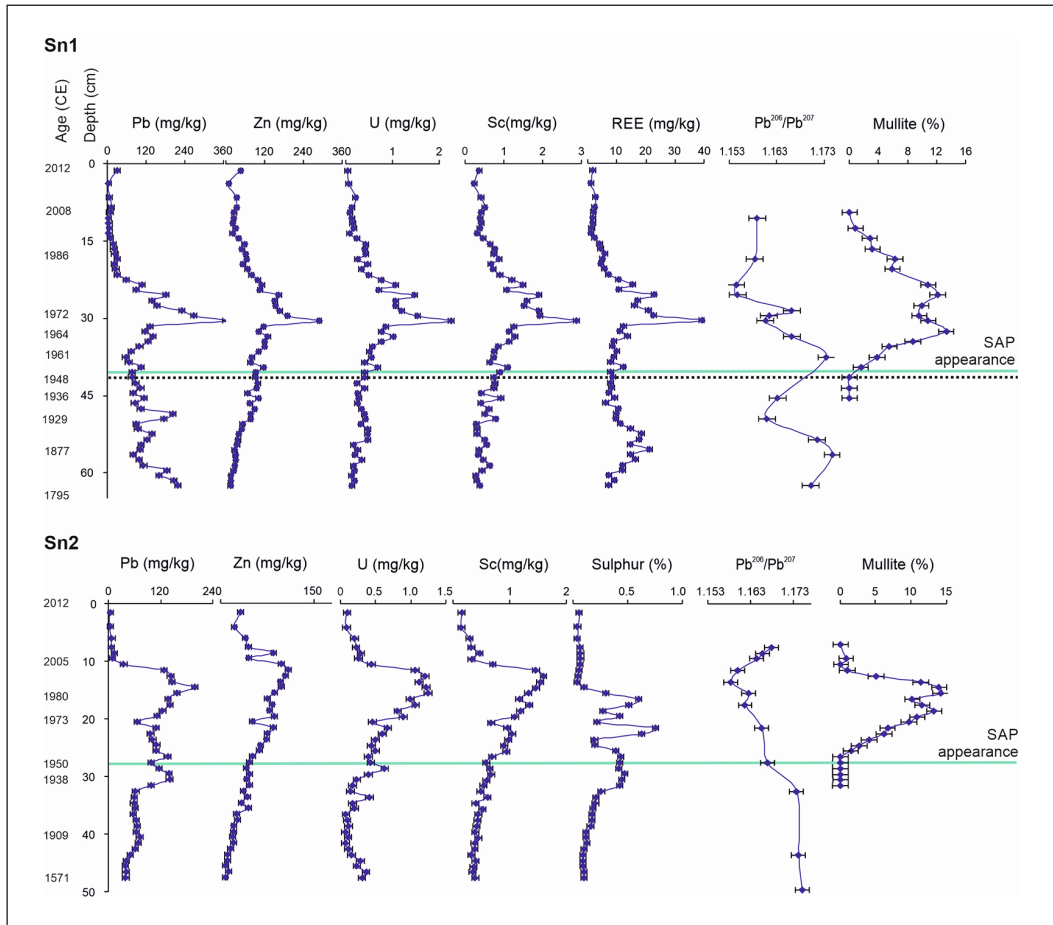


Figure 3. Comparison of  $^{239+240}\text{Pu}$  and  $^{137}\text{Cs}$  versus CF/CS modelled dates in Sn0 and Sn I.



**Figure 4.** Geochemistry of Sn1 and Sn2 (based on Fiałkiewicz-Kozieł et al., 2020 except for mullite and sulphur). Sn1 profile records the appearance of 1952-Pu and spheroidal aluminosilicates (SAP) signal, while Sn2 SAP signal only. The chronology is based on the  $^{14}\text{C}/^{210}\text{Pb}$  model. At a depth of 41.5 cm (Sn1), the date of the first Pu appearance is provided, not measured in Sn2. Reproduced in colour in online version.

### Trace elements (Sn1, Sn2)

The contents of Pb, Zn, Cu, Ni, Cr, Sr, Ti and Al in Sn1 and Sn2 cores, as well as REE in Sn1 core, were first discussed in Fiałkiewicz-Kozieł et al. (2020), where all elements represented a similar pattern of distribution. Further discussion in the current paper is centred on Pb, Zn, U, Sc, Al, REE and S (Figure 4) for their well-documented linkages with anthropogenic activity and the ability for long-range atmospheric transport (Steinnes and Friedland, 2006). Pb, Zn and U are known to be released by industrial processes (De Vleeschouwer et al., 2010a; Shotyky et al., 1998), S was an important component of acid rain (Mylona, 1996), while Sc, Al and REE carry the information on dust supply to the peatland (Kylander et al., 2007; Shotyky et al., 2001). For better profile documentation, only concentrations are shown in the figures. However, it should be mentioned that it is crucial to calculate accumulation rates using the age-depth model and bulk density values for a better interpretation of observed variability in the concentrations. Normalised results allow for excluding the effect of some post-depositional processes in the peatland.



Regarding chemical composition, the Sn1 profile was divided into two layers. From ~62.5 to 45.5 cm (1795–1952 CE) – with an increase of Pb concentration – up to 220 mg/kg (62.5; 49.5 cm). A slight increase of Zn is observed from 59.5 cm (1828 CE). An increase in REE is observed from 52.5 to 57.5 cm (Figure 4).

In Sn2, despite partial disturbance of the investigated profile, the distinction of the two layers is also possible (Figure 4). According to the age-depth model, the layer spanning period similar to Sn1 and Sn0 is 43.5 cm (1899 CE) to the top of the profile. The increase in Pb and S is observed from 31.5 cm (1937 CE), and a slight rise is distinguished in U concentration (33.5 cm – 1928 CE).

### Hg (Sn0)

In the Sn0 core, mercury concentration (Figure 8) shows a gradual increase from around 70 ng/g at the core base to the maximum level of 228 ng/g in 30.5 cm (1966 CE) and then declines upwards to a value of over 40 ng/g, with some minor fluctuations (Figure 8). A significant 1950s upturn in Hg concentration is observed at 36.5 cm (1953 CE).

### Pb isotopes (Sn1, Sn2)

Pb isotopic ratios are presented in Figure 4. In both Sn1 and Sn2 profiles,  $^{206}\text{Pb}/^{207}\text{Pb}$  altered from more to less radiogenic value, reaching 1.160–1.162 during the time of the highest detected concentration of all elements. The ash content and chronology revealed disturbances and hiatuses in Sn2. However, the 27.5–0 cm layer, the most important for the Anthropocene, seems reliable and coherent. Lead isotopic signatures revealed similar age and depth patterns in peat profiles during the last 100 years. The observed more complex pattern of Pb isotopic signature in Sn1 might be due to different, higher resolution data, which show variations linked to different sources of Pb associated with changes in wind direction.

### C, N, $\delta^{13}\text{C}$ , $\delta^{15}\text{N}$ (Sn0)

The TOC, TN,  $\delta^{13}\text{C}$  and  $\delta^{15}\text{N}$  values are shown in Figure 8. With depth, there is a long-term enrichment in  $^{13}\text{C}$  as shown by the  $\delta^{13}\text{C}$  values (from about  $-24\text{‰}$  to  $-28.5\text{‰}$ ), but from the surface to the first 8 cm there is a  $^{13}\text{C}$  depletion ( $-25.7\text{‰}$  to  $-28.5\text{‰}$ ).  $\delta^{15}\text{N}$  values also show a long-term enrichment from around  $-7\text{‰}$  to  $-1\text{‰}$  in the oldest part of the core. TOC values remain constant with depth while TN values show a significant decrease in the first 8 cm. TN values show a significant drop from 1.2 to 0.4 in the first 8 cm and then fluctuate between 0.4 and 1. C:N ratios increase in the first 8 cm from 35 to 90 and then fluctuate between 90 and 40.

### Technofossils

SCP (Sn0). The SCPs appeared in the record at 44–45 cm (approximately  $1939 \pm 7$  CE) (Figure 8) and occurred continuously above 42–43 cm ( $1943 \pm 7$  CE) to 8–9 cm ( $2012 \pm 1$  CE). No SCPs were found in the upper 8 cm of the core.

SAP (Sn0, Sn1, Sn2). Spheroidal aluminosilicates fly ash particles (SAP) were the dominant technogenic dust particles detected in the profiles using SEM. In Sn0, SAPs were first found at a depth of 44.5 cm ( $1939 \pm 7$  CE) (Figure 8), in Sn1 at 39.5 cm ( $1950 \pm 4$  CE) and in Sn2 at 26.5 cm (1950 CE) (Figure 4). The size of SAP was analysed for the Sn0 and Sn1 profiles. Most of the SAP at different depths were  $<1\text{--}9.5\ \mu\text{m}$ , which indicates the predominance of SAPs from long-range transport

(Smieja-Król and Fiałkiewicz-Kozieł, 2014). A mean SAP size of  $2.2\mu\text{m}$  was obtained for Sn0 ( $n=300$ ) and  $2.4\mu\text{m}$  ( $n=180$ ) in Sn1. A small number ( $<2\%$ ) of much larger ( $10\text{--}50\mu\text{m}$ ), less regular and highly porous technogenic aluminosilicates found within a depth range of  $35\text{--}25\text{cm}$  in Sn1 (1961–1983 CE) were probably from local sources. Mullite, an aluminosilicate ( $\text{Al}_6\text{Si}_2\text{O}_{13}$ ) by-product of coal combustion in high temperatures ( $>1100^\circ\text{C}$ ; Smieja-Król et al., 2019), was detected in all profiles (Figures 4, 7 and 8) using XRD. In Sn0, mullite was detected between  $12.5$  and  $40.5\text{cm}$  (1947 and 2003 CE), with elevated contents between  $21.5$  and  $35.5\text{cm}$  (1955 and 1988 CE) and a maximum at  $26.5\text{cm}$ . In Sn1, the range of mullite occurrence was similar, between  $11.5$  and  $39.5\text{cm}$  (1952 and 2005 CE), with two distinct maxima at  $25.5$  and  $32.5\text{cm}$ . In Sn2, the mullite was only identified in a relatively narrow depth range between  $9$  and  $26\text{cm}$ . The two maxima were at  $15\text{--}16$  and  $18\text{--}19\text{cm}$ .

### Biotic proxies (Sn1)

The biostratigraphy was based on pollen, non-pollen palynomorphs, microcharcoal and testate amoebae (Sn1) (Figures 5 and 6). The proxies revealed three main ecological phases of the peatland with different local and regional agricultural and pastoral activities.

Pollen spectra revealed alpine and upper montane forests in the vicinity of the Śnieżka coring sites. Alpine vegetation was represented by the predominance of herbaceous plants (Poaceae) and high shares of *Pinus sylvestris*, *Betula alba* and *Picea abies*. The upper montane forest was indicated by *Pinus mugo* pollen grains. High values of Cerealia type indicate enhanced agricultural activity in the mountain valleys (Figure 5). In terms of the Anthropocene, the most pronounced changes in vegetation are marked by the decline of coprophilous fungi percentages and a gradual increase in *Urtica* values. The decline of coprophilous fungi indicates a decline in pastoral activity. In contrast, the increase in *Urtica* pollen percentages may be linked to further nitrification of peatland from the input of industrial dust. From ca. 1956 CE ( $37.5\text{cm}$ ), a continuous presence of pollen of *Ambrosia artemisiifolia* type was observed (Figure 5). The microcharcoal analysis revealed a pronounced upturn at  $49.5\text{cm}$  (1927 CE), keeping the increasing trend till  $19.5\text{cm}$  (1995 CE).

Regarding the testate amoebae, the continuous high abundance of the mixotrophic species *Archerella flavum* and *Hyalosphenia papilio* were observed till  $37.5\text{cm}$  (1956 CE). This was followed by the disappearance of mixotrophs at  $36.5\text{cm}$  ( $1959 \pm 3$  CE) and the appearance of dry habitat indicators such as *Alabasta militaris*, *Nebela tinctoria* and *Galeripora catinus* (drop in the water table, mean DWT value:  $26\text{cm}$ ) was recognised (Figure 6).

The shift between biotic proxies is clearly visible in the non-metric multidimensional scaling (NMDS)'s ordination space (Figure 9). The most significant variables influencing the communities have been water table depth ( $\text{Pr}( > r )$ : 0.001), Fe ( $\text{Pr}( > r )$ : 0.022) and Pb ( $\text{Pr}( > r )$ : 0.095). The communities typical for the lower part of the peat core were characterised by high abundances of mixotrophic testate amoebae, and the peatland possessed high water tables. Among geochemical data, the presence of Fe and Pb is connected to this phase. The shift in the data set appeared between ca. 1951 and 1965 CE, and the anthropogenically affected communities were dominated by heterotrophic testate amoeba species. The water table decreased, and plant communities were dominated by *Ambrosia* and *Urtica*.

## Discussion

### Peat record before 1950 and preferred base for the Anthropocene series

The obtained multi-proxy data of Sn0, Sn1 and Sn2 profiles allows distinction of the boundary between the Holocene and the proposed Anthropocene series encompassing the period

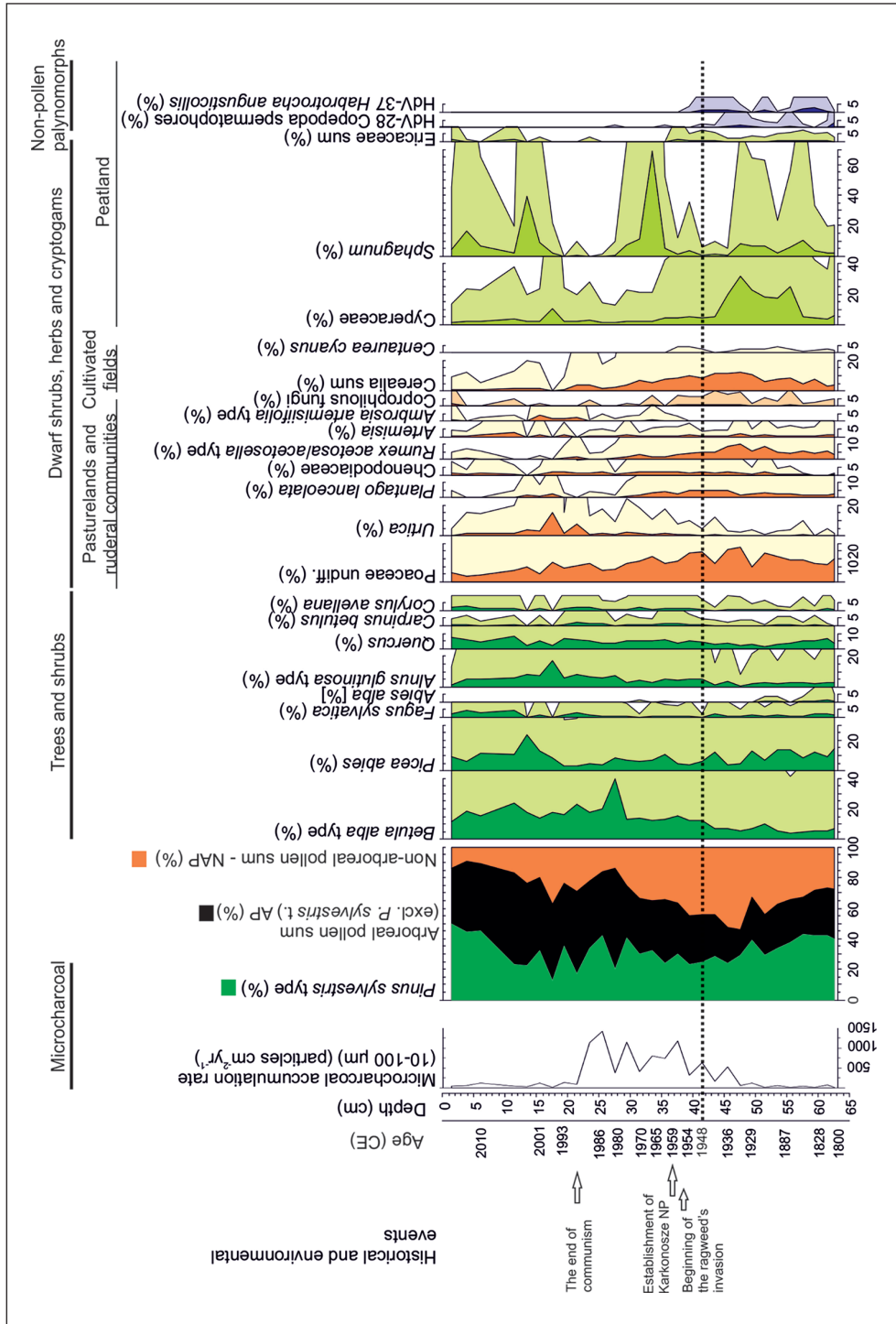


**Figure 5.** Simplified pollen diagram for Sn I profile. 10 × exaggeration provided for better visualisation. At a depth of 41.5 cm, the date of the first Pu appearance is provided. Reproduced in colour in online version.

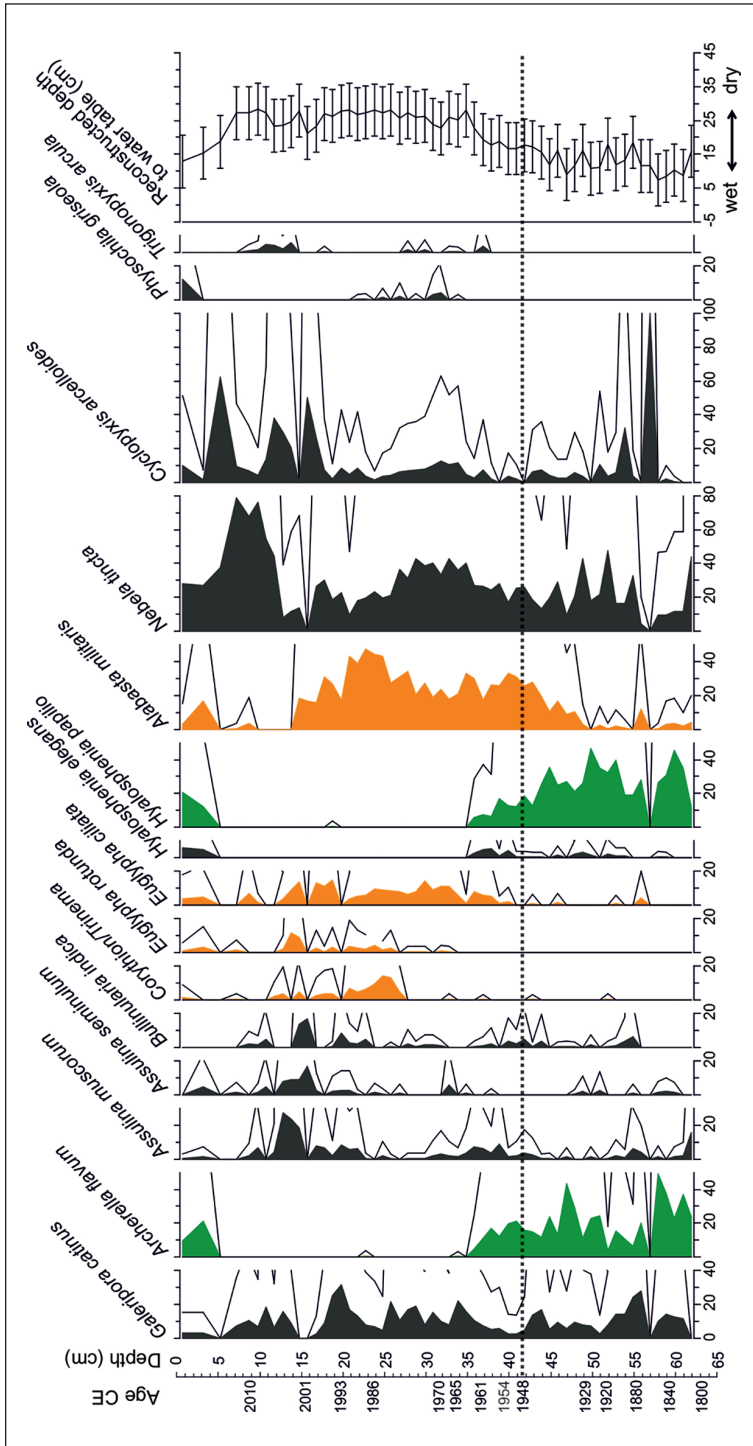


**Figure 6.** Short percentage diagram of the most frequent testate amoebae and reconstructed depth to the water table in Sn I profile. In green – mixotrophs, orange – indicators of dry conditions. 5 × exaggeration provided for better visualisation. At a depth of 41.5 cm, the date of the first Pu appearance is provided. Reproduced in colour in online version.

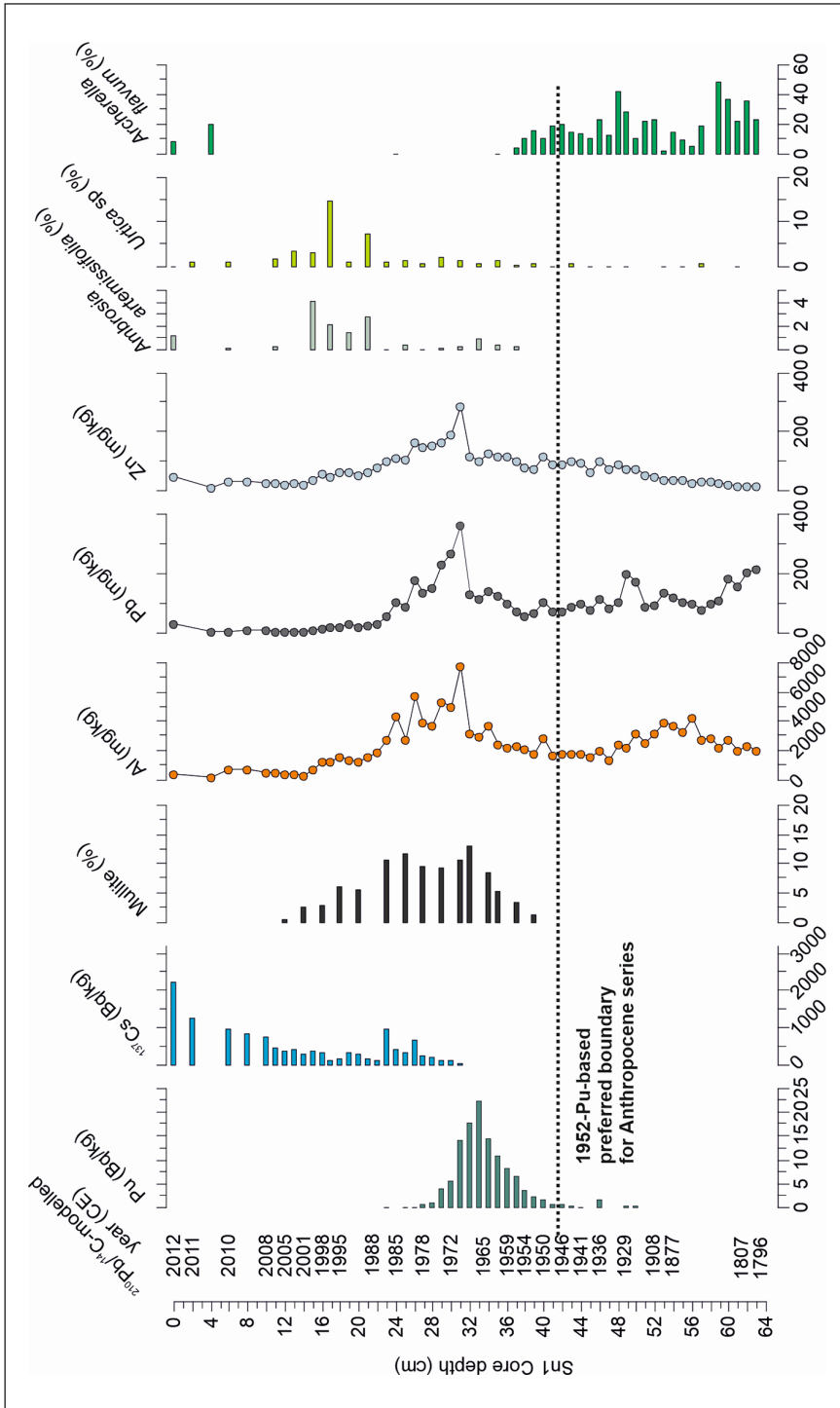


**Figure 7.** Summary of the most significant markers in S n1. The horizontal dashed line is referred to first global Pu fallout (1952). Reproduced in colour in online version.

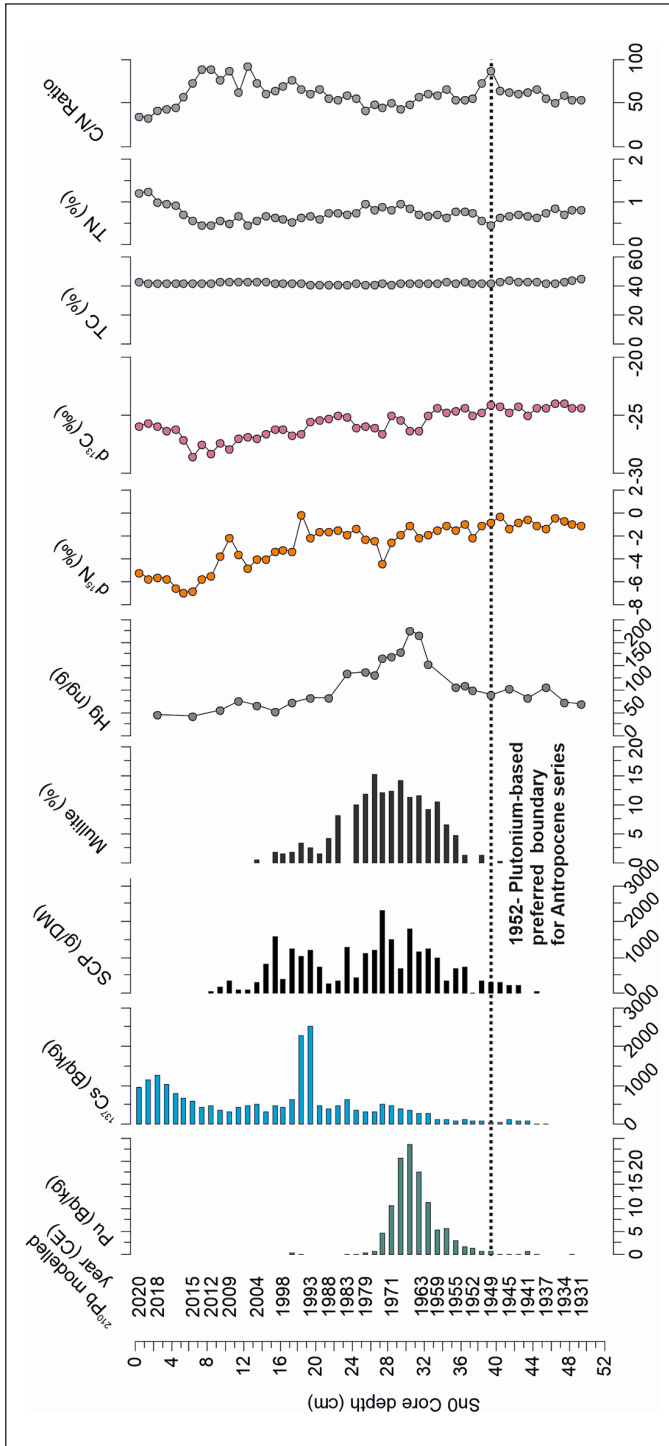


**Figure 8.** Summary of markers in Sn0. The horizontal dashed line is referred to first global Pu fallout (1952). Reproduced in colour in online version.



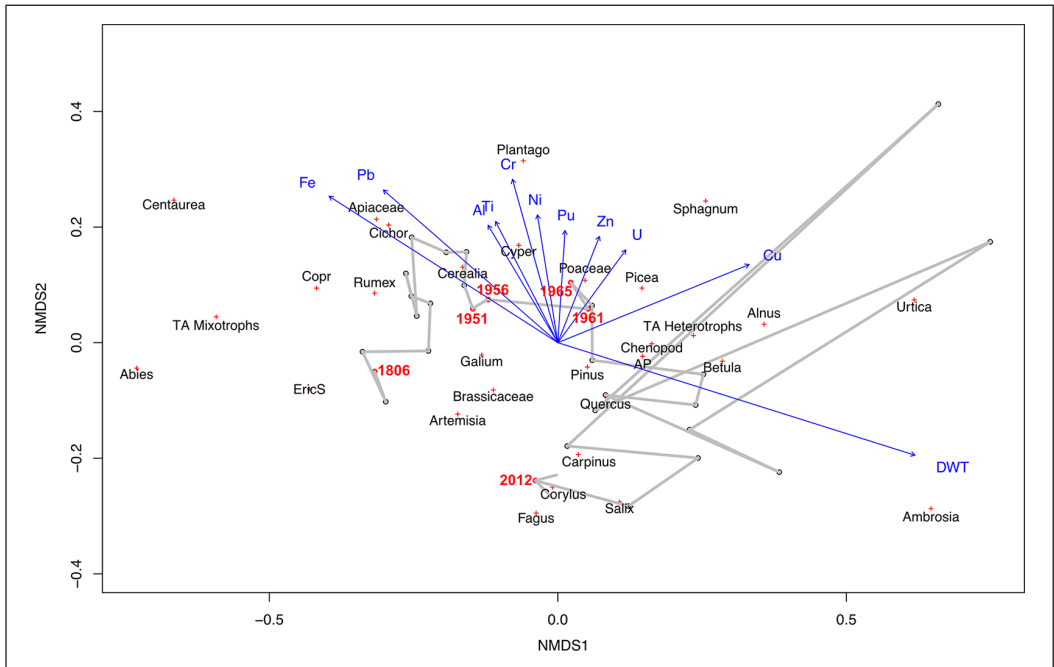


**Figure 9.** Non-metric multidimensional scaling (NMDS) diagrams for Śnieżka multiproxy dataset. NMDS shows a low-stress value (0.106) for the two-dimensional solution. Reconstructed depth to the water table (DWT) and geochemical data are projected on the ordination space. Codes for pollen types follow the pollen diagram (Figure 5). Testate amoebae are projected as a sum of mixotrophic species ('TA Mixotrophs') and a sum of heterotrophic species ('TA Heterotrophs'). Reproduced in colour in online version.

of overwhelming human pressure on the environment, called the Anthropocene. Geochemical and palaeoecological data consistently indicate that the period between 1795 and  $1948 \pm 4$  CE (63.5–41.5 cm – for Sn1 and 47.5–26.5 cm – for Sn2) was characterised by moderate industrial activity in the region. This is confirmed by relatively low Pb accumulation rates (8–20 mg/m<sup>2</sup>/year), accompanying high concentrations of Pb in peat (100–220 mg/kg in Sn1) as well as less radiogenic Pb isotopic signatures (1.174–1.160). Zn concentrations were low, albeit displaying an increasing trend during this period and only at the end of the 19th century (around 1897 CE; 52.5 cm) was a considerable increase in Zn accumulation rate from 2.5 to 7 mg/m<sup>2</sup>/year. From pollen data, it emerged that the Sudetes mountains were prone to intensifying deforestation, although the predominant land use type was arable farming and pastoralism. The low fluxes of microcharcoal (60 particles/cm<sup>2</sup>/year) (Figure 5) seem to indicate low emissions of combustion-related dust but also low settlement density in adjacent valleys and submontane zones, which might affect the appearance of the fire indicator in the peat record (Patterson et al., 1987). Testate amoebae composition (Figure 6), with high shares of mixotrophic species *Archerella flavum* or *Hyalosphenia papilio* provided evidence for wet conditions (i.e. higher groundwater level) in the mire.

The year  $1948 \pm 4$  CE (the first global Pu fallout in 1952) appears to be a tipping point in the Śnieżka peatland history (Figures 7–9). In the three cores, this date is marked by sharp changes in the deposition of multiple independent geochemical markers of diverse human activities such as fossil fuel combustion, industrialisation and nuclear weapon tests superimposed on climatically driven environmental changes. The first worldwide appearance of Pu (Koide et al., 1979; Krey,

1967; UNSCEAR, 2000) can be recognised globally in different natural archives, including peatlands (Waters et al., 2015). Owing to its synchronicity, Pu is considered a primary marker of the onset of the Anthropocene (Head et al., 2022; Waters et al., 2018).

The appearance of Pu is accompanied by the pronounced inflexion (acceleration) or significant upturn of other chemostratigraphic and selected biostratigraphic indicators as well as technogenic particles (SCP, SAP and mullite), which appeared in the pre-Anthropocene deposits as traces. The NMDS solution (Figure 9) showed low stress values (0.1060076) and proved that the shift in testate amoeba groups (mixotrophs vs. heterotrophs), plant macrofossils and main pollen types appeared in the 1950s, further supporting this period as the boundary for the Anthropocene series. The markers, crucial in presenting global patterns in the geological record, were divided into three globally identified categories, that is, primary markers, technogenic impacts and climate change, represented here by specific, regional examples of indicators.

### Primary markers

The atmospheric deposition of  $^{239+240}\text{Pu}$  in the Śnieżka cores correlates with global events in the history of radioactive fallout, notably coupled to thermonuclear atmospheric weapons testing from 1952 and the Partial Test Ban Treaty signed in 1963 (Figures 3, 7 and 8). Plutonium isotopes ( $^{238,239,240}\text{Pu}$ ) are useful independent chronostratigraphic markers due to long half-lives of 24,100 ( $^{239}\text{Pu}$ ) and 6561 years ( $^{240}\text{Pu}$ ), respectively. They are characterised by low solubility and high stability in peatlands, as Pu is retained by *Sphagnum* mosses (Testa et al., 1999; Waters et al., 2015). There is a 2-cm difference between the first appearance of  $^{239+240}\text{Pu}$  in Sn1 and Sn0, caused by different dynamics of peat growth. Nevertheless, the high repeatability between the two profiles confirms the immobility of Pu in the presented stratigraphic record (Figures 3, 7 and 8). We may summarise that the highest extended peak of  $^{239+240}\text{Pu}$  activity concentrations dated to  $1965 \pm 3$  CE for Sn1 and  $1966 \pm 5$  CE for Sn0 (CF/CS) were the consequences of the most intensive period of nuclear weapons testing and a further moratorium in the 1960s.

Due to Pu immobility, the historical data of the first global fallout should be attributed to the layer of 1952 CE, which is consistent with ages modelled by the  $^{210}\text{Pb}$  method.

1952-peaks are observed at the 41.5 cm depth ( $1948 \pm 4$  CE) for Sn1 and 39.5 cm depth ( $1949 \pm 6$  CE) for Sn0 (Figures 3–6, Supplemental Table 1). Below 1952 in both profiles, we observed small peaks dated 1941 for Sn0 and 1936 for Sn1. The presence of the global fallout derived Pu at depth-ages preceding 1952 is probably evidence of the post-depositional migration of Pu vertically downwards, also observed by others in peat profiles (Kazakevičiūtė-Jakučiūnienė et al., 2022; Quinto et al., 2013). However, the extent of the mobility is much smaller than for Cs, thus not significantly affecting the age-depth models based on Pu profiles. The shift in the levels of the  $\text{F}^{14}\text{C}$  for Sn0 (Figure 10) compared with the atmospheric curve NH1 (Hua et al., 2022) revealed a great similarity to the Pu curve plotted versus  $^{210}\text{Pb}$  model, confirming the robustness of the used modelling.

The peaks of  $^{239,240}\text{Pu}$  in Sn0 and Sn1 profiles also correspond well with the main peaks of  $^{137}\text{Cs}$  (Figure 3).

The peak concentrations of  $^{137}\text{Cs}$  are slightly shifted in depth with respect to the peaks of plutonium. In profile Sn1, the maximum of the  $^{137}\text{Cs}$  activity is observed in the top layer, which could be attributed to the active uptake by living plants (e.g. Mróz et al., 2017; Rosén et al., 2009). However, the Chernobyl peak (1986) of  $^{137}\text{Cs}$  is partly preserved. Profil Sn0 is less affected by plant uptake of Cs, which corresponds with a less dense plant cover at the Sn1 sampling site. Also, the Chernobyl peak is more distinct. Measurable  $^{137}\text{Cs}$  activity was found in all layers of both profiles, pointing to the downward mobility of Cs. The mobility of  $^{137}\text{Cs}$  in ombrotrophic peat bogs

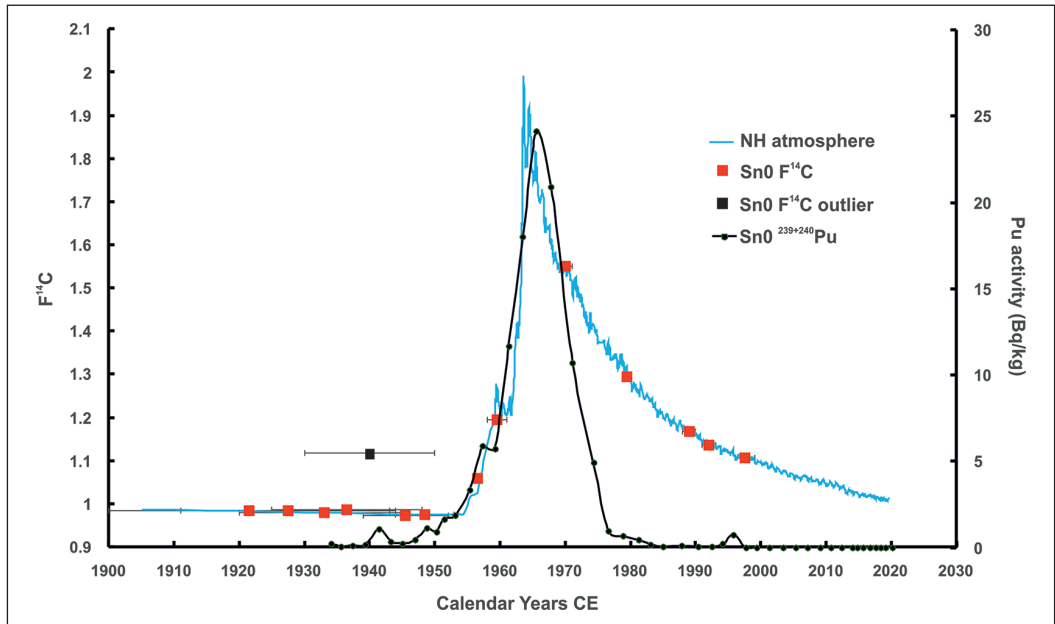


**Figure 10.** The comparison of  $F^{14}\text{C}$  values (Sn0) (against  $^{14}\text{C}$  age-depth model) with atmospheric curve and with Pu, which is presented against  $^{210}\text{Pb}$  model. The overall similarity revealed between two independent models has confirmed the accuracy and robustness of both methods of dating. Reproduced in colour in online version.

(Olid et al., 2008; Zaccone et al., 2007) is due to the lack of suitable mineral particles for the adsorption of alkali metal cations like Cs.

Some vertical mobility of  $^{137}\text{Cs}$  in ombrotrophic peat deposits is demonstrated in Sn0 and Sn1 and is also observed in other sites (e.g. Fiałkiewicz-Kozieł et al., 2014; Kazakevičiūtė-Jakučiūnienė et al., 2022; MacKenzie et al., 1997; Mitchell and McDonald, 1992; Mróz et al., 2017; Rosén et al., 2009).  $^{137}\text{Cs}$  could be immobile (Li et al., 2017; van der Plicht et al., 2013; Łokas et al., 2013) or partially mobile downward and upward in the peat profile (Schell et al., 1989) due to biological activity in the root zone and changing water table (Aaby et al., 1979; Rosén et al., 2009). Nevertheless, it was possible to recognise the most characteristic events of radionuclide fallout, that is, Chernobyl accident.

### *The technogenic impact: Synchronous increases of chemical elements concentration and associated appearance of SCP and SAP, mullite, $\delta^{15}\text{N}$ and $\delta^{13}\text{C}$*

The increased global human population and their energy demands have induced a dramatic increase in the number of power plants, industrial facilities, car use and associated fossil fuel combustion (Waters et al., 2016, 2018). Fossil fuel-based power plants and industrial activities emit flue gases and fly-ashes (e.g. Jones et al., 2012; Vassilev et al., 2001). These are transported in the atmosphere before they are deposited on aquatic and terrestrial surfaces, including different natural archives.

Ombrotrophic peatlands are among the best archives of rare and trace elements deposition due to being fed only from the atmosphere and the effective immobilisation of selected elements, once deposited, which can be interpreted against an age-depth function (De Vleeschouwer et al., 2010a;

Shotyk, 1988). In Śnieżka peatland, trace elements were determined in Sn1 and Sn2, but the simultaneous increase in ash content of Sn1 and Sn2, which correlates with peaks in element concentrations, also allows for the recognition of such a layer in ash content in Sn0. Hence, Sn0 ash content may be considered equivalent to chemical element deposition and, in particular, corresponds with the profile of mercury content and accumulation (Figure 8).

**Trace elements.** Pb and Zn are representative of industrial activity and so may be used in the discussion regarding markers for the Anthropocene series. Numerous studies have identified ombrotrophic bogs as among the best Pb archives due to their exclusive input via deposition from the atmosphere (e.g. Shotyk and Le Roux, 2005; Shotyk et al., 1998). Pb always accompanies Zn in peat because of their co-occurrence in ore deposits (De Vleeschouwer et al., 2009; Smieja-Król et al., 2010; Fiałkiewicz-Kozieł et al., 2018). Despite its mobility in peatlands (Weiss et al., 2007), Zn deposition shows similar patterns to Pb in the Śnieżka cores (Figure 4; Fiałkiewicz-Kozieł et al., 2020).

Comparison of industrially driven Pb deposition in archives from different countries and continents indicates regional or local differences due to the individual history of industrial development (Longman et al., 2020). However, despite significant intracontinental variability, the most pronounced increase, observed in the mid-20th century, has been statistically confirmed (Longman et al., 2020). This has important implications for determining a clear boundary for the Anthropocene series using trace elements. While peat sequences in different countries may show varying dates for the onset of trace metal contamination and for peak metal concentrations making them unsuitable as a global synchronous marker, the rise in trace metal inputs for Pb and Zn in the 1950s does appear to be globally synchronous for all studied peat deposits. This increase in almost all investigated trace elements and REE is visible in Śnieżka peatland (Fiałkiewicz-Kozieł et al., 2020) and here may be attributed to lignite combustion in ‘Black Triangle’ countries (Fiałkiewicz-Kozieł et al., 2015, 2020). The 1950s acceleration in Pb is observed in different environmental archives, for example, in Czechia (Novak et al., 2008), Scotland (Farmer et al., 1997), Greenland (Shotyk et al., 2003), but also China (Bao et al., 2015; Fiałkiewicz-Kozieł et al., 2022) and Kyrgyzstan (Grigholm et al., 2016). This ‘Great Acceleration’ in chemical element inputs due to increased industrial activity is given here as one of the significant markers of the proposed Anthropocene.

**Technofossils.** High-temperature coal combustion also produces technofossils like spheroidal carbonaceous particles (SCP) or fly ash spheroidal aluminosilicates (SAP), easily detected in peat profiles (Fiałkiewicz-Kozieł et al., 2020; Rose, 2015; Smieja-Król and Fiałkiewicz-Kozieł, 2014; Swindles et al., 2015 – for this study). SCPs and SAPs appeared for the first time in western Europe in the mid-19th century, but the marked global increase in abundance is observed around 1950 CE, with peak inputs to archives ranging regionally from the 1970s to the 1990s (Rose, 2015; Smieja-Król et al., 2019). The link with specific technology, developed in the late 19th century and boosted in the 1950s–1960s allows for the determination of distinct boundaries in the geological record, even at remote sites far from industrial centres (Fiałkiewicz-Kozieł et al., 2016, 2022).

In Śnieżka, the first appearance is observed in 1940 CE; however, a significant upturn is visible in the 1950s (Figures 7 and 8).

**Stable isotopes.** Stable carbon ( $\delta^{13}\text{C}_{\text{TOC}}$ ) and nitrogen ( $\delta^{15}\text{N}$ ) isotope signatures can, with some limitations, also be used to show the anthropogenic contribution of carbon and nitrogen deposition on the Śnieżka peatland. Both  $\delta^{13}\text{C}_{\text{TOC}}$  and  $\delta^{15}\text{N}$  displayed similar patterns (Pearson correlation coefficient  $r=0.72$ ,  $p < 0.001$ ), indicating that the same environmental factors control them.

Decreasing trends in  $\delta^{13}\text{C}$  and  $\delta^{15}\text{N}$  between the early 1940s CE and 1970s CE reflect a long-term depletion in atmospheric  $^{13}\text{C}$  and  $^{15}\text{N}$ . For  $\text{CO}_2$ , the decrease could act as a manifestation of the so-called Suess effect, a worldwide reduction of atmospheric  $\delta^{13}\text{C}_{\text{CO}_2}$  values by  $\sim 2\%$  within the last 200 years due to the burning of fossil fuels (Keeling, 1979; Keeling et al., 1979). The  $\delta^{13}\text{C}_{\text{TOC}}$  and  $\delta^{15}\text{N}$  trend could indicate that between the 1940s and 1970s CE, there occurred a decline in  $\delta^{13}\text{C}$  and  $\delta^{15}\text{N}$  values in atmospheric  $\text{CO}_2$  and  $\text{NO}_3$ , respectively, in the Sudetes.

It should be emphasised that  $\delta^{13}\text{C}_{\text{OM}}$  and  $\delta^{15}\text{N}$  are known to be strongly influenced by microbial OM degradation, leaching and re-fixation in the peat acrotelm, which preferentially removes light C and N isotopes, thus leading to an increase of  $\delta^{13}\text{C}_{\text{OM}}$  and  $\delta^{15}\text{N}$  in the residual recalcitrant material (Esmeijer-Liu et al., 2012). On the other hand, it has been documented that in the early stages of a microbial attack,  $^{13}\text{C}$  enriched carbohydrates are removed and as a result, the  $\delta^{13}\text{C}$  of the remaining organic material is shifted towards lower values (Meyers, 1997). Such an effect is presumably responsible for stable C isotope signatures in the uppermost 8 cm-thick layers of the Sn cores (Figure 8).

### Biotic markers of the Anthropocene series

**Pollen analysis.** The critical changes in elements and technofossils at the proposed Holocene/Anthropocene transition correspond with pronounced ecological changes mirrored by pollen and testate amoebae in the Sn1 profile (Figures 5–7). However, while chemical markers and technofossils often have worldwide distributions, the pollen-inferred delimitation of the Anthropocene relies on species that represent region-specific ecological trends (Deza-Araujo et al., 2022). Therefore, representative analogues should be selected from different parts of the globe when comparing these markers. Globalisation phenomena and climate change have altered the distribution of non-native species, which have become invasive in new environments (Storkey et al., 2014). In Europe, one of the best-known alien plants is *Ambrosia artemisiifolia* L. (common ragweed), which has expanded over Europe since 1940 CE due to its contamination within crop seeds and transboundary transport (Chauvel et al., 2006; Storkey et al., 2014). From the Sn1 core, it emerges that in central Europe, *Ambrosia artemisiifolia* appeared in  $1956 \pm 3$  CE (Figure 5).

An interesting feature of the Sn0 profile was a gradual increase in *Urtica* pollen abundance, which might be an effect of enrichment with nitrogen. A decline in nitrogen input occurred due to the cessation of pastoral activity connected with the establishment of Karkonosze National Park in 1959. However, in the following period, intensified tourism and enhanced atmospheric fallout caused by industrial development in the Black Triangle (Kmieć et al., 1995; Myśków et al., 2019) partially compensated for this N loss. *Urtica dioica* and *Urtica urens* are characteristic representatives of nitrophilic weeds (Rosnitschek-Schimmel, 1983) and *Urtica* sp. records show an increasing trend from 1950, representative of many European mountain records (Segnana et al., 2020), and a clear connection between its presence and the anthropogenic phase (Figure 9).

In the Snieżka record, it is also clear that in ca. 1960 CE, there was a considerable change in the microbial food web reflected by the disappearance of mixotrophic testate amoebae (Figure 6). This change is found to reflect the broader tendency observed in some parts of the Northern Hemisphere: Siberia (Lamentowicz et al., 2015) and Canada (van Bellen et al., 2018) as well as in the Southern Hemisphere (e.g. van Bellen et al., 2016). In all these locations, the collapse in mixotrophic species was associated with the lowering of the water table and shading by shrubs (Creedy et al., 2018; Heal, 1964; Lamentowicz and Mitchell, 2005; Lamentowicz et al., 2020; Marcisz et al., 2014; Payne et al., 2016; Schönborn, 1965). Even though global warming was among the most important drivers of the peatland drying trend during the past 70 years (Gallego-Sala et al., 2018; Swindles et



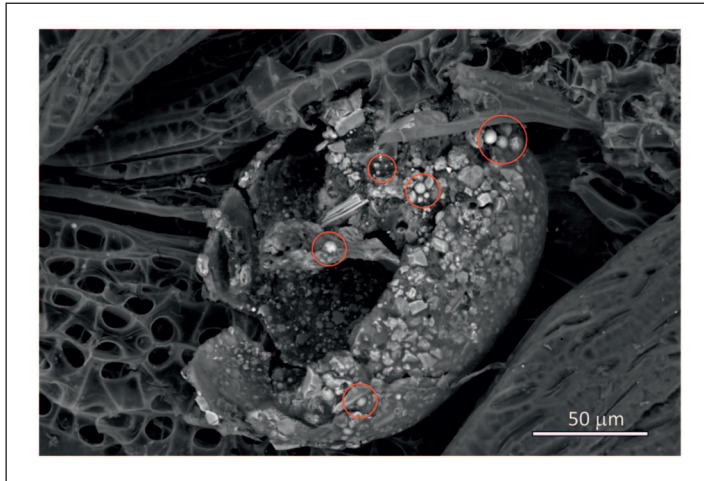


**Figure 11.** Fossil shell of a testate amoeba with SAP built into the shell (indicated by red circles) (Sn0, depth 25–26 cm). Reproduced in colour in online version.

al., 2019), there are alternative reasons for the disappearance of mixotrophs in the Śnieżka bog. It appears that the local testate amoebae communities were exposed to fly ash deposition originating from intense industrial activity around the so-called Black Triangle (Figure 1), and it has been hypothesised that this dust harmed mixotrophic metabolism and eliminated communities living at the capitula of *Sphagnum* (Fiałkiewicz-Kozieł et al., 2015; Marcisz et al., 2020). Synergistic effects of air pollution and anthropogenic global warming might cause the worldwide extinction of the populations of mixotrophs in *Sphagnum* peatlands in the future (Loisel et al., 2021). By contrast, the Śnieżka peatland has also been identified as the location of new ecotypes of testate amoebae which are resistant to pollution and which use fly-ash particles to build their shells (Figure 11). The first evidence for this phenomenon was described in the Izery mountains (Fiałkiewicz-Kozieł et al., 2015).

### Śnieżka peatland as potential GSSP

Due to the widespread environmental effects of industrial activity in the Black Triangle and the high-resolution record preserved in the peatland, the Śnieżka site seems significant for documenting the Anthropocene. The unique feature of the site lies in its location in the subalpine zone and at the trajectory of air masses carrying pollutants over long distances across Europe. The Anthropocene series in the Sn cores is clearly distinguished by the distributions of Pu isotopes, technofossils (SCP, SAP and mullite) as well as trace metals, all of which are synchronous with other Anthropocene records worldwide.

As a candidate for a GSSP representative Anthropocene core, the Sn0 has the following advantages:

- It displays a robust age model obtained using  $^{210}\text{Pb}$  and verified by independent markers ( $^{137}\text{Cs}$ ,  $\text{F}^{14}\text{C}$ )
- It is characterised by a relatively high peat accumulation rate (0.66 cm/year on average) which provides a high-resolution geological record (around 2 years per 1 cm) and thus



allows for the identification of a distinct boundary between the Holocene and Anthropocene series

- The Sn0 peat profile provides a continuous geological record for the last c.a. 100 years (i.e. no hiatuses, gaps and other disturbances were identified)
- The Sn0 Anthropocene archive encompasses a wide array of critical markers such as plutonium radionuclides, fly ash particles, Hg and stable C and N isotopes which are consistent with the previously studied well-documented Sn1 profile
- The Śnieżka site is located in a protected area of the National Park and is easily accessible for further studies. Access to the peatland is facilitated thanks to proximity to touristic tracks, although permission for collecting peat material, given by the Ministry of Climate and Environments and the National Park Administration, is mandatory.

The main disadvantages of the proposed stratotype include the lack of annual lamination and the lack of a lithological marker at the proposed level.

## Conclusions

The Śnieżka peat profile provides a significant thickness of deposited organic matter and presents a comprehensive dataset of markers which can be used to distinguish a 1950s boundary between the Holocene and Anthropocene series. Despite an absence of annual layering the proposed GSSP core has a well-constrained chronology and key markers (Pu, Cs, technofossils) can be correlated to adjacent cores. Importantly, further analysis is required to repeat some crucial measurements undertaken in 2020–2022 as part of future examinations of the candidate GSSP core. The proposed name for the stage/age-level is Sudetian.

## Acknowledgements

Marcin Siepak and Jolanta Dopieralska are thanked for measurements published in previous study (Fiałkiewicz-Kozieł et al., 2020). We would like to acknowledge the Haus der Kulturen der Welt (HKW, Berlin) for collaborating with the Anthropocene Working Group in the assessment of the candidate GSSP-sites. The collaboration was established in the framework of HKW's long-term initiative Anthropocene Curriculum, an international project for experimental forms of Anthropocene research and education developed by HKW and the Max Planck Institute for the History of Science (MPIWG, Berlin) since 2013. Gael Le Roux is thanked for the discussion about Pu mobility. Colin Waters is warmly thanked for all constructive comments.

## Declaration of conflicting interests

The author(s) declared no potential conflicts of interest with respect to the research, authorship, and/or publication of this article.

## Funding

The author(s) disclosed receipt of the following financial support for the research, authorship, and/or publication of this article: This research was funded by the Polish National Centre of Science (NCN) 2011/01/D/ST10/02579 granted to BFK as well as by IGIG, Adam Mickiewicz University funds for scientific activity. We would like to acknowledge the Haus der Kulturen der Welt (HKW, Berlin) for collaborating with the Anthropocene Working Group in the assessment of the candidate GSSP-sites. The collaboration was established in the framework of HKW's long-term initiative Anthropocene Curriculum, an international project for experimental forms of Anthropocene research and education developed by HKW and the Max Planck Institute for the History of Science (MPIWG, Berlin) since 2013.

## ORCID iDs

B Fiałkiewicz-Kozieł  <https://orcid.org/0000-0003-0369-985X>

I Hajdas  <https://orcid.org/0000-0003-2373-2725>

## Supplemental material

Supplemental material for this article is available online.

## References

- Aaby B, Jacobsen J and Jacobsen OS (1979) Pb-210 dating and lead deposition in the ombrotrophic peat bog Draved Mose Denmark. *Danmarks Geologisk Ungersoglse Arbog*, pp. 5–43.
- Appleby PG, Shotyk W and Fankhauser A (1997) Lead-210 age dating of three peat cores in the Jura Mountains, Switzerland. *Water Air & Soil Pollution* 100: 223–231.
- AWG (2020) Newsletter of the Anthropocene working group, vol. 10. Subcommission on Quaternary Stratigraphy (International Commission on Stratigraphy), AWG. Available at <http://quaternary.stratigraphy.org/wp-content/uploads/2021/03/AWG-Newsletter-2020-Vol-10.pdf>
- Bao K, Shen J, Wang G, et al. (2015) Atmospheric deposition history of trace metals and metalloids for the last 200 years recorded by three peat cores in Great Hinggan Mountain Northeast China. *Atmosphere* 6(3): 380–409.
- Bińczycycki T, Weber J, Mielnik L, et al. (2020) Lead isotope ratios in podzol profiles as a tracer of pollution source in the subalpine zone of the Karkonosze National Park Sudety MTS (south-western Poland). *CATENA* 189: 104476.
- Bronk Ramsey C (2009) Bayesian analysis of radiocarbon dates. *Radiocarbon* 51(1): 337–360.
- Chauvel B, Dessaint F, Cardinal-Legrand C, et al. (2006) The historical spread of *Ambrosia artemisiifolia* L. in France from herbarium records. *Journal of Biogeography* 33: 665–673.
- Creevy AL, Andersen R, Rowson JG, et al. (2018) Testate amoebae as functionally significant bioindicators in forest-to-bog restoration. *Ecological Indicators* 84: 274–282.
- Cwanek A, Łokas E, Mitchell EAD, et al. (2021) Temporal variability of Pu signatures in a <sup>210</sup>Pb-dated sphagnum peat profile from the northern Ural Russian Federation. *Chemosphere* 281: 130962.
- De Vleeschouwer F, Chambers FM and Swindles GT (2010b) Coring and sub-sampling of peatlands for palaeoenvironmental research. *Mires and Peat* 7: 1.
- De Vleeschouwer F, Fagel N, Cheburkin A, et al. (2009) Anthropogenic impacts in North Poland over the last 1300 years – A record of Pb, Zn, Cu, Ni and S in an ombrotrophic peat bog. *The Science of the Total Environment* 407: 5674–5684.
- De Vleeschouwer F, Le Roux G and Shotyk W (2010a) Peat as an archive of atmospheric pollution and environmental change: A case study of lead in Europe. *PAGES* 18: 20–22.
- Deza-Araujo M, Morales-Molino C, Conedera M, et al. (2022) Influence of taxonomic resolution on the value of anthropogenic pollen indicators. *Vegetation History and Archaeobotany* 31: 67–84.
- Esmeyjer-Liu AJ, Kürschner WM, Lotter AF, et al. (2012) Stable carbon and nitrogen isotopes in a peat profile are influenced by early stage diagenesis and changes in atmospheric CO<sub>2</sub> and N deposition. *Water Air & Soil Pollution* 223: 2007–2022.
- Farmer JG, Mackenzie AB, Sugden CL, et al. (1997) A comparison of the historical lead pollution records in peat and freshwater lake sediments from central Scotland. *Water Air & Soil Pollution* 100: 253–270.
- Fiałkiewicz-Kozieł B, Bao K and Smieja-Król B (2022) Geographical drivers of geochemical and mineralogical evolution of Motianling peatland (Northeast China) exposed to different sources of rare earth elements and Pb Nd and Sr isotopes. *The Science of the Total Environment* 807: 150481.
- Fiałkiewicz-Kozieł B, De Vleeschouwer F, Mattielli N, et al. (2018) Record of Anthropocene pollution sources of lead in disturbed peatlands from southern Poland. *Atmospheric Environment* 179: 61–68.
- Fiałkiewicz-Kozieł B, Kołaczek P, Piotrowska N, et al. (2014) High-resolution age-depth model of a peat bog in Poland as an important basis for paleoenvironmental studies. *Radiocarbon* 56: 109–125.
- Fiałkiewicz-Kozieł B, Łokas E, Gałka M, et al. (2020) Influence of transboundary transport of trace elements on mountain peat geochemistry (Sudetes Central Europe). *Quaternary Science Reviews* 230: 106162.

- Fiałkiewicz-Kozieł B, Smieja-Król B, Frontasyeva M, et al. (2016) Anthropogenic- and natural sources of dust in peatland during the Anthropocene. *Scientific Reports* 6: 38731.
- Fiałkiewicz-Kozieł B, Smieja-Król B, Ostrovnya TM, et al. (2015) Peatland microbial communities as indicators of the extreme atmospheric dust deposition. *Water Air & Soil Pollution* 226: 97–103.
- Gallagher D, McGee EJ and Mitchell PI (2001) A recent history of  $^{14}\text{C}$ ,  $^{137}\text{Cs}$ ,  $^{210}\text{Pb}$  and  $^{241}\text{Am}$  accumulation at two Irish peat bog sites: An east versus west coast comparison. *Radiocarbon* 43(2B): 517–525.
- Gallego-Sala AV, Charman DJ, Brewer S, et al. (2018) Latitudinal limits to the predicted increase of the peatland carbon sink with warming. *Nature Climate Change* 8: 907–913.
- Givelet N, Le Roux G, Cheburkin A, et al. (2004) Suggested protocol for collecting handling and preparing peat cores and peat samples for physical chemical mineralogical and isotopic analyses. *Journal of Environmental Monitoring* 6: 481–492.
- Glina B and Bogacz A (2012) Concentration and pools of trace elements in organic soils in the Izera Mountains. *Journal of Elementology* 18(2): 199–209.
- Grigholm B, Mayewski PA, Aizen V, Kreutz K, Wake CP, Aizen E, Kang S, Maasch KA, Handley, M.J., Sneed, S.B. (2016) Mid-twentieth century increases in anthropogenic Pb, Cd and Cu in central Asia set in hemispheric perspective using Tien Shan ice core. *Atmospheric Environment* 131: 17–28.
- Grübler A (2002) *Trends in Global Emissions: Carbon, Sulphur and Nitrogen*. Laxenburg, Austria: IIASA, pp.35–53.
- Hajdas I (2008) Radiocarbon dating and its applications in Quaternary studies. *Quaternary Science Journal - Eiszeitalter und Gegenwart* 57(1/2): 2–24.
- Hansson SV, Claustres A, Probst A, et al. (2017) Atmospheric and terrigenous metal accumulation over 3000 years in a French mountain catchment: Local vs distal influences. *Anthropocene* 19: 45–54.
- Head MJ, Steffen W, Fagerlind D, et al. (2022) The Great Acceleration is real and provides a quantitative basis for the proposed Anthropocene Series/Epoch. *Episodes* 45(4): 359–376.
- Heal OW (1964) Observations on the seasonal and spatial distribution of Testacea (Protozoa: Rhizopoda) in Sphagnum. *Journal of Animal Ecology* 33: 395–412.
- Hua Q, Turnbull JC, Santos GM, et al. (2022) Atmospheric radiocarbon for the period 1950–2019. *Radiocarbon* 64: 723–745.
- Jones KB, Ruppert LF and Swanson SM (2012) Leaching of elements from bottom ash economizer fly ash and fly ash from two coal-fired power plants. *International Journal of Coal Geology* 94: 337–348.
- Julkowska V (2016) Cultural heritage as the heritage of memory. *Historia a teoria* 1: 7–9.
- Kajukało K, Fiałkiewicz-Kozieł B, Gałka M, et al. (2016) Abrupt ecological changes in the last 800 years inferred from a mountainous bog using testate amoebae traits and multi-proxy data. *European Journal of Protistology* 55: 165–180.
- Kazakevičiūtė-Jakučiūnienė L, Tarasiuk N, Maceika E, et al. (2022) Analysis of the vertical distribution of  $^{137}\text{Cs}$  and  $^{239,240}\text{Pu}$  in waterlogged and non-boggy soils by the sequential extraction method. *Journal of Environmental Radioactivity* 253-254: 106990.
- Keeling CD (1979) The Suess effect:  $^{13}\text{C}$ - $^{14}\text{C}$  interrelations. *Environment International* 2: 229–300.
- Keeling CD, Mook WG and Tans PP (1979) Recent trends in the  $^{13}\text{C}/^{12}\text{C}$  ratio of atmospheric carbon dioxide. *Nature* 277: 121–123.
- Kmieć G, Kacperczyk K, Zwozdziaż A, et al. (1995) Acid pollutants in air and precipitation/deposition at the Sudeten Mountains, Poland. *Water Air & Soil Pollution* 85: 2131–2136.
- Koide M, Michel R, Goldberg ED, et al. (1979) Depositional history of artificial radionuclides in the Ross Ice Shelf Antarctica. *Earth and Planetary Science Letters* 44: 205–223.
- Kolář T, Čermák P, Oulehle F, et al. (2015) Pollution control enhanced spruce growth in the “Black Triangle” near the Czech–Polish border. *The Science of the Total Environment* 538: 703–711.
- Krey PW (1967) Atmospheric burnup of a plutonium-238 generator. *Science* 158: 769–771.
- Kylander ME, Muller J, Wüst RA, et al. (2007) Rare earth element and Pb isotope variations in a 52 kyr peat core from Lynch’s crater (NE Queensland Australia): Proxy development and application to paleoclimate in the southern hemisphere. *Geochimica et Cosmochimica Acta* 71: 942–960.

- Lamentowicz M, Kajukalo-Drygalska K, Kołaczek P, et al. (2020) Testate amoebae taxonomy and trait diversity are coupled along an openness and wetness gradient in pine-dominated Baltic bogs. *European Journal of Protistology* 73: 125674.
- Lamentowicz M and Mitchell EA (2005) The ecology of testate amoebae (Protists) in *Sphagnum* in north-western Poland in relation to peatland ecology. *Microbial Ecology* 50: 48–63.
- Lamentowicz M, Słowiński M, Marcisz K, et al. (2015) Hydrological dynamics and fire history of the last 1300 years in western Siberia reconstructed from a high-resolution ombrotrophic peat archive. *Quaternary Research* 84: 312–325.
- Li C, Le Roux G, Sonke J, et al. (2017) Recent  $^{210}\text{Pb}$ ,  $^{137}\text{Cs}$  and  $^{241}\text{Am}$  accumulation in an ombrotrophic peatland from Amsterdam Island (Southern Indian Ocean). *Journal of Environmental Radioactivity* 175–176: 164–169.
- Loisel J, Gallego-Sala AV, Amesbury MJ, et al. (2021) Author correction: Expert assessment of future vulnerability of the global peatland carbon sink. *Nature Climate Change* 11: 362–377.
- Loisel J, Yu Z, Beilman DW, et al. (2014) A database and synthesis of northern peatland soil properties and Holocene carbon and nitrogen accumulation. *The Holocene* 24(9): 1028–1042.
- Łokas E, Mietelski JW, Ketterer ME, et al. (2013) Sources and vertical distribution of  $^{137}\text{Cs}$ ,  $^{238}\text{Pu}$ ,  $^{239+240}\text{Pu}$  and  $^{241}\text{Am}$  in peat profiles from southwest Spitsbergen. *Applied Geochemistry* 28: 100–108.
- Longman J, Ersek V and Veres D (2020) High variability between regional histories of long-term atmospheric Pb pollution. *Scientific Reports* 10: 20890.
- Luciano E (2022) Is ‘Anthropocene’ a suitable chronostratigraphic term? *Anthropocene Science* 1: 29–41.
- MacKenzie AB, Farmer JG and Sugden CL (1997) Isotopic evidence of the relative retention and mobility of lead and radiocaesium in Scottish ombrotrophic peats. *The Science of the Total Environment* 203(2): 115–127.
- MacKenzie AB, Logan EM, Cook GT, et al. (1998) Distributions inventories and isotopic composition of lead in  $^{210}\text{Pb}$ -dated peat cores from contrasting biogeochemical environments: Implications for lead mobility. *The Science of the Total Environment* 223(1): 25–35.
- Magiera T, Żogała B, Szuszkiewicz M, et al. (2019) Combination of different geophysical techniques for the location of historical waste in the Izery Mountains (SW Poland). *The Science of the Total Environment* 682: 226–238.
- Marcisz K, Jassey VEJ, Kosakyan A, et al. (2020) Testate Amoeba functional traits and their use in paleoecology. *Frontiers in Ecology and Evolution* 8: 340.
- Marcisz K, Lamentowicz L, Słowińska S, et al. (2014) Seasonal changes in sphagnum peatland testate amoeba communities along a hydrological gradient. *European Journal of Protistology* 50: 445–455.
- Mazurski KR (1986) The destruction of forests in the Polish Sudetes mountains by industrial emissions. *Forest Ecology and Management* 17: 303–315.
- Meyers PA (1997) Organic geochemical proxies of paleoceanographic, paleolimnologic, and paleoclimatic processes. *Organic Geochemistry* 27: 213–250.
- Miśka K, Urban G, Tomczyński K (2016) Long-term air temperature variation in the Karkonosze mountains according to atmospheric circulation. *Theoretical and Applied Climatology* 125: 337–351.
- Millar DJ, Cooper DJ, Dwire KA, et al. (2017) Mountain peatlands range from  $\text{CO}_2$  sinks at high elevations to sources at low elevations: Implications for a changing climate. *Ecosystems* 20: 416–432.
- Mitchell G and McDonald AT (1992) Discolouration of water by peat following induced drought and rainfall simulation. *Water Research* 26(3): 321–326.
- Mróz T, Łokas E, Kocurek J, et al. (2017) Atmospheric fallout radionuclides in peatland from Southern Poland. *Journal of Environmental Radioactivity* 175–176: 25–33.
- Mylona S (1996) Sulphur dioxide emissions in Europe 1880–1991 and their effect on sulphur concentrations and depositions. *Tellus B* 48(5): 662–689.
- Myśkow E, Błaś M, Sobik M, et al. (2019) The effect of pollutant fog deposition on the wood anatomy of subalpine Norway spruce. *European Journal of Forest Research* 138: 187–201.
- Němec M, Wacker L and Gäggeler H (2010) Optimization of the graphitization process at age-1. *Radiocarbon* 52(3): 1380–1393.

- Novak M, Brizova E, Adamova M, et al. (2008) Accumulation of organic carbon over the past 150 years in five freshwater peatlands in western and central Europe. *The Science of the Total Environment* 390(2–3): 425–436.
- Olid C, Garcia-Orellana J, Martínez-Cortizas A, et al. (2008) Role of surface vegetation in  $^{210}\text{Pb}$ -dating of peat cores. *Environmental Science & Technology* 42: 8858–8864.
- Patterson WA, Edwards KJ and Maguire DJ (1987) Microscopic charcoal as a fossil indicator of fire. *Quaternary Science Reviews* 6: 3–23.
- Payne RJ, Creevy A, Malysheva E, et al. (2016) Tree encroachment may lead to functionally-significant changes in peatland testate amoeba communities. *Soil Biology and Biochemistry* 98: 18–21.
- Pech P, Wojtuń B, Samecka-Cymerman A, et al. (2022) Metals in plant functional types of ombrotrophic peatlands in the Sudetes (SW Poland). *Archives of Environmental Contamination and Toxicology* 82: 506–519.
- Popowski B (2005) Results of a palynological analysis of peat sediments from Izerskie Bagno (Izerskie mts). *Acta Botanica Silesiaca* 2: 95–106.
- Quinto F, Hrncsek E, Krachler M, et al. (2013) Determination of  $^{239}\text{Pu}$ ,  $^{240}\text{Pu}$ ,  $^{241}\text{Pu}$  and  $^{242}\text{Pu}$  at femtogram and attogram levels – Evidence for the migration of fallout plutonium in an ombrotrophic peat bog profile. *Environmental Science Processes & Impacts* 15(4): 839–847.
- Rangwala I and Miller JR (2012) Climate change in mountains: A review of elevation-dependent warming and its possible causes. *Climatic Change* 114: 527–547.
- Reimer PJ, Brown TA and Reimer RW (2004) Discussion: Reporting and calibration of post-bomb  $^{14}\text{C}$  data. *Radiocarbon* 46(3): 1299–1304.
- Rose NL (1994) A note on further refinements to a procedure for the extraction of carbonaceous fly-ash particles from sediments. *Journal of Paleolimnology* 11(2): 201–204.
- Rose NL (2015) Spheroidal carbonaceous fly ash particles provide a globally synchronous stratigraphic marker for the Anthropocene. *Environmental Science & Technology* 49(7): 4155–4162.
- Rosén K, Vinichuk M and Johanson KJ (2009)  $^{137}\text{Cs}$  in a raised bog in central Sweden. *Journal of Environmental Radioactivity* 100(7): 534–539.
- Rosnitschek-Schimmel I (1983) Biomass and nitrogen partitioning in a perennial and an annual nitrophilic species of *Urtica*. *Zeitschrift für Pflanzenphysiologie* 109(3): 215–225.
- Schell WR, Tobin MJ and Massey CD (1989) Evaluation of trace metal deposition history and potential element mobility in selected cores from peat and wetland ecosystems. *Science of the Total Environment* 87: 19–42.
- Schönborn W (1965) Untersuchungen über die zoochlorellen-symbiose der Hochmoor-testaceen. *Limnologia (Berlin)* 3: 173–176.
- Segnana M, Oeggl K, Poto L, et al. (2020) Holocene vegetation history and human impact in the eastern Italian alps: A multi-proxy study on the Coltrondo peat bog Comelico Superiore Italy. *Vegetation History and Archaeobotany* 29: 407–426.
- Shotyk W (1988) Review of the inorganic geochemistry of peats and peatland waters. *Earth-Science Reviews* 25(2): 95–176.
- Shotyk W, Cheburkin AK, Appleby PG, et al. (1998) Lead in three peat bog profiles Jura Mountains Switzerland: Enrichment factors isotopic composition and chronology of atmospheric deposition. *Water, Air, and Soil Pollution* 100(3–4): 297–310.
- Shotyk W, Goodsite ME, Roos-Barraclough F, et al. (2003) Anthropogenic contributions to atmospheric Hg, Pb, and As deposition recorded by peat cores from Greenland and Denmark dated using the  $^{14}\text{C}$  AMS “bomb pulse curve”. *Geochimica et Cosmochimica Acta* 67: 3991–4011.
- Shotyk W and Le Roux G (2005) Biogeochemistry and cycling of lead. *Metal Ions in Biological Systems* 43: 240–275.
- Shotyk W, Weiss D, Kramers JD, et al. (2001) Geochemistry of the peat bog at Etang de la Gruère Jura mountains Switzerland and its record of atmospheric Pb and lithogenic trace metals (Sc Ti Y Zr and REE) since 12370  $^{14}\text{C}$  yr BP. *Geochimica et Cosmochimica Acta* 65(14): 2337–2360.



- Skrzypek G, Baranowska-Kącka A, Keller-Sikora A, et al. (2009) Analogous trends in pollen percentages and carbon stable isotope composition of Holocene peat—Possible interpretation for palaeoclimate studies. *Review of Palaeobotany and Palynology* 156(3–4): 507–518.
- Smieja-Król B and Fiałkiewicz-Kozieł B (2014) Quantitative determination of minerals and anthropogenic particles in some Polish peat occurrences using a novel SEM point-counting method. *Environmental Monitoring and Assessment* 186: 2573–2587.
- Smieja-Król B, Fiałkiewicz-Kozieł B, Michalska A, et al. (2019) Deposition of mullite in peatlands of southern Poland: Implications for recording large-scale industrial processes. *Environmental Pollution* 250: 717–727.
- Smieja-Król B, Fiałkiewicz-Kozieł B, Sikorski J, et al. (2010) Heavy metal behaviour in peat – A mineralogical perspective. *The Science of the Total Environment* 408(23): 5924–5931.
- Sobik M, Błaś M, Migala M, et al. (2014) Klimat. In: Knapik R and Raj A (eds) *Przyroda Karkonoskiego Parku Narodowego* [Karkonoski Park Narodowy]. Jelenia Góra, Bielsko-Biała: DIMOGRAF, pp.147–186.
- Speranza A, Hanke J, van Geel B, et al. (2000) Late-Holocene human impact and peat development in the černá Hora bog, Krkonoše Mountains, Czech Republic. *The Holocene* 10: 575–585.
- Steinnes E and Friedland AJ (2006) Metal contamination of natural surface soils from long-range atmospheric transport: Existing and missing knowledge. *Environmental Review* 14(3): 169–186.
- Storkey J, Stratonovitch P, Chapman DS, et al. (2014) A process-based approach to predicting the effect of climate change on the distribution of an invasive allergenic plant in Europe. *PLoS ONE* 9: 101371.
- Strzyszczyk Z and Magiera T (2001) Record of industrial pollution in Polish ombrotrophic peat bogs. *Physics and Chemistry of the Earth Part A Solid Earth and Geodesy* 26(11–12): 859–866.
- Swindles GT, Morris PJ, Mullan DJ, et al. (2019) Widespread drying of European peatlands in recent centuries. *Nature Geoscience* 12: 922–928.
- Swindles GT, Watson E, Turner TE, et al. (2015) Spheroidal carbonaceous particles are a defining stratigraphic marker for the Anthropocene. *Scientific Reports* 5: 10264.
- Synal HA, Stocker M and Suter M (2007) MICADAS: A new compact radiocarbon AMS system. *Nuclear Instruments & Methods in Physics Research Section B-Beam Interactions With Materials and Atoms* 259(1): 7–13.
- Testa C, Jia G, Degetto S, et al. (1999) Vertical profiles of  $^{239,240}\text{Pu}$  and  $^{241}\text{Am}$  in two sphagnum mosses of Italian peat. *The Science of the Total Environment* 232(1–2): 27–31.
- Turetsky MR, Kotowska A, Bubier J, et al. (2014) A synthesis of methane emissions from 71 northern temperate and subtropical wetlands. *Global Change Biology* 20(7): 2183–2197.
- UNSCEAR (2000) Exposure from man-made sources of radiation. Report volume 1: Sources, Annex C.
- Urban G and Tomczyński K (2017) Air temperature trends at Mount śnieżka (Polish Sudetes) and solar activity, 1881–2012. *Acta Geographica Slovenica* 57(2): 33–44.
- Urban NR, Eisenreich SJ, Grigal DF, et al. (1990) Mobility and diagenesis of Pb and  $^{210}\text{Pb}$  in peat. *Geochimica et Cosmochimica Acta* 54(12): 3329–3346.
- Valde-Novak P (1999) *Początki Osadnictwa w Sudetach*. Instytut Archeologii i Etnologii PAN, Kraków, p.238. (In Polish With English Summary).
- van Bellen S, Magnan G, Davies L, et al. (2018) Testate amoeba records indicate regional 20th-century lowering of water tables in ombrotrophic peatlands in central-northern Alberta, Canada. *Global Change Biology* 24: 2758–2774.
- van Bellen S, Mauquoy D, Hughes PD, et al. (2016) Late-Holocene climate dynamics recorded in the peat bogs of Tierra del Fuego South America. *The Holocene* 26: 489–501.
- van der Plicht J, Yeloff D, van der Linden M, et al. (2013) Dating recent peat accumulation in European ombrotrophic bogs. *Radiocarbon* 55(3): 1763–1778.
- Vassilev SV, Greta M, Eskenazy GM, et al. (2001) Behaviour of elements and minerals during preparation and combustion of the Pernik coal Bulgaria. *Fuel Processing Technology* 72: 103–129.
- Wardenaar EPC (1987) A new hand tool for cutting peat profiles. *Canadian Journal of Botany* 65: 1772–1773.
- Waters CN, Syvitski JPM, Gałuszka A, et al. (2015) Can nuclear weapons fallout mark the beginning of the Anthropocene Epoch? *Bulletin of the Atomic Scientists* 71(3): 46–57.



- Waters CN, Turner SD, Zalasiewicz J, et al. (2023) Candidate sites and other reference sections for the Global boundary Stratotype Section and Point (GSSP) of the Anthropocene series. *The Anthropocene Review* 10(1): 3–24 (in this issue).
- Waters CN, Zalasiewicz J, Summerhayes C, et al. (2016) The Anthropocene is functionally and stratigraphically distinct from the Holocene. *Science* 351: 137.
- Waters CN, Zalasiewicz J, Summerhayes C, et al. (2018) Global Boundary Stratotype Section and Point (GSSP) for the Anthropocene series: Where and how to look for potential candidates. *Earth-Science Reviews* 178: 379–429.
- Weiss DJ, Rausch N, Mason TFD, Colesa BJ, Wilkinson JJ, Ukonmaanaho L, Arnold T, Nieminen, TM (2007) Atmospheric deposition and isotope biogeochemistry of zinc in ombrotrophic peat. *Geochimica et Cosmochimica Acta* 71(14): 3498–3517.
- Wojtuń B (2006) *Peat Mosses (Sphagnaceae) in Mires of the Sudetes Mountains (SW Poland): A Floristic and Ecological Study*. Wrocław-Poznań: University of Agriculture, p.225.
- Wojtuń B, Samecka-Cymerman A, Kolon K, et al. (2018) Metals in *Racomitrium lanuginosum* from Arctic (SW Spitsbergen Svalbard archipelago) and alpine (Karkonosze SW Poland) tundra. *Environmental Science and Pollution Research* 25: 12444–12450.
- Woźniak Z (1970) *Osadnictwo Celtyckie witalic Polsce*. Wrocław, Ossolineum (in Polish).
- Xu J, Morris PJ, Liu J, et al. (2018) PEATMAP: Refining estimates of global peatland distribution based on a meta-analysis. *CATENA* 160: 134–140.
- Yu ZC (2012) Northern peatland carbon stocks and dynamics: A review. *Biogeosciences* 9(10): 4071–4085.
- Zaccone C, Coccozza C, Cheburkin AK, et al. (2007) Enrichment and depletion of major and trace elements, and radionuclides in ombrotrophic raw peat and corresponding humic acids. *Geoderma* 141(3–4): 235–246.
- Zuna M, Mihaljevič M, Šebek O, et al. (2011) Recent lead deposition trends in the Czech Republic as recorded by peat bogs and tree rings. *Atmospheric Environment* 45(28): 4950–4958.